Environmental Technology & Innovation 25 (2022) 102076

Contents lists available at ScienceDirect

Environmental Technology & Innovation

journal homepage: www.elsevier.com/locate/eti

Cyclohexane and benzene separation by fixed-bed adsorption on activated carbons prepared from coconut shell

Aniyohana Valencia [a], Roberto Muñiz-Valencia [a,b], Silvia G. Ceballos-Magaña [c], Cintia Karina Rojas-Mayorga [a], Adrian Bonilla-Petriciolet [d], Jorge González [a], Ismael Alejandro Aguayo-Villarreal [a,*]

[a] Universidad de Colima, Facultad de Ciencias Químicas, Km 9 carretera Colima-Coquimatlán, C.P. 28400, Coquimatlán, Colima, Mexico
[b] Centro de Investigación en Recursos Naturales y Sustentabilidad, Universidad Bernardo O'Higgins, Fabrica 1990, Segundo Piso, Santiago, Chile
[c] Universidad de Colima, Facultad de Ciencias, Bernal Díaz del Castillo 340, C.P. 28045, Colima, Mexico
[d] Instituto Tecnológico de Aguascalientes, Aguascalientes 20256, Mexico

ARTICLE INFO

Article history:
Received 12 July 2021
Received in revised form 20 October 2021
Accepted 31 October 2021
Available online 2 November 2021

Keywords:
Activated carbon
Benzene
Cyclohexane
Competitive adsorption

ABSTRACT

New activated carbons were prepared from coconut shell and tested to evaluate their adsorption properties to separate benzene and cyclohexane. A Taguchi experimental design was utilized to identify the best preparation conditions of the activated carbons based on their benzene adsorption capacities. Type and concentration of the chemical agent, ratio of precursor mass/chemical agent volume and physical activation time were the variables analyzed. Adsorbents were physiochemically characterized and the adsorption capacities of these adsorbents were evaluated in a dynamic system coupled to a GC-FID. Benzene and cyclohexane adsorption capacities of tested adsorbents ranged from 1.35 to 51.40 and 0.49 to 25.20 mmol/g, respectively. The statistical analysis indicated that the activating agent, impregnation ratio, and physical activation time were the most important variables to prepare an activated carbon with a high benzene adsorption during the binary mixture separation. In particular, the adsorbents obtained with $ZnCl_2$ showed the highest adsorption properties. The best activated carbon showed an acceptable separation of 92.64% of benzene and 7.36%: of cyclohexane and a reuse efficiency of 96% after four adsorption/desorption cycles. This study contributes with new findings on the preparation of low-cost and effective activated carbons for the separation of benzene and cyclohexane at industrial level.

1. Introduction

Volatile organic compounds (VOCs) are a range of chemical compounds that includes aliphatic and aromatic hydrocarbons, alcohols, aldehydes, ketones, esters and halogenated compounds. They have different physicochemical properties but share the same volatility characteristic. Many VOCs are of interest to the chemical industry; for example, hydrocarbons are used to produce fuels (gasoline, diesel, natural gas), car lubricants, detergents, and plastic products. Particularly, benzene and cyclohexane are the most valuable hydrocarbons processed in the petrochemical industry. Cyclohexane is used in the

* Corresponding author.
E-mail address: alejandro_1017@hotmail.com (I.A. Aguayo-Villarreal).

https://doi.org/10.1016/j.eti.2021.102076

synthesis of adipic acid and caprolactam, which are raw precursors for nylon (Li et al., 2018; Sun et al., 2018). The demand for this polymer in the thermoplastic industry is growing at about 6% annually; hence, cyclohexane consumption is also increasing. Around 54% of its production is used in the synthesis of adipic acid for nylon-6/6, 39% is used in the fabrication of caprolactam for nylon-6 and 7% is used to produce dissolvents, insecticides, and plasticizers (Dada and Achenie, 2012). About 80%–85% of the cyclohexane produced worldwide is obtained from the catalytic hydrogenation of benzene (Li et al., 2018), a reaction that produces a mixture of cyclohexane and residual benzene, whereby the unreacted benzene must be removed (Salleh et al., 2017). Due to their close boiling points (0.6 °C difference), they can form an azeotropic mixture and thus their separation is one of the most difficult in the petrochemical industry. Besides, the conventional methods used for their separation (azeotropic and extractive distillation) present several disadvantages such as process complexity, high operating costs, use of dissolvents, and high energy consumption (Ribeiro et al., 2012; Salleh et al., 2018; Wang et al., 2008).

Accordingly, the research trend consists in the development of economically workable and environmentally friendly separation methods. In this context, adsorption is a separation method of simple operation, low operating cost, and high efficiency that is also useful when considering the recovery of valuable VOCs for industry (Guo et al., 2016; Wang et al., 2015a). During adsorption, a compound of interest adheres to the surface of the adsorbent due to different interactions (e.g., electrostatic and van der Waals forces, hydrogen bond, covalent or ionic bonds) that occur between them. In this sense, there is a great variety of adsorbents with different physicochemical properties such as activated carbons, zeolites, silica gels, activated aluminas, polymeric resins, carbon nanotubes, pillared clays, ordered mesoporous silicas, and metal–organic frameworks (MOF), among others (Zhang et al., 2019; Lu et al., 2018; Son et al., 2016; Yang, 2003).

In particular, activated carbon is a carbon-rich adsorbent characterized by its porous structure, large surface area, hydrophobic properties, thermo-stability, high adsorption capacity, and low production cost that makes it as an ideal adsorbent to separate chemical compounds (Zhang et al., 2017; Pak et al., 2016). Activated carbon can be manufactured from a plethora of feedstocks (Ahmedna et al., 2000). However, the use of organic wastes has been preferred to decrease the feedstock costs and environmental problems (González-García, 2018). For the manufacturing of activated carbon, it is important to consider that both the precursor (waste chemical composition) and the preparation conditions will determine the surface characteristics (pore structure, pore size distribution, pore-volume, surface area, and surface functional groups), chemical composition, quality, and economic viability (Ahmedna et al., 2000; Ahmad et al., 2014).

There are several methods to produce activated carbon from organic waste, aiming to generate porous materials with different surface chemistry. These methods generally consist of two main steps; the first is the carbonization of the precursor (organic waste) under an inert or reducing (N_2, H_2) atmosphere at a moderate temperature (600–800 °C); the second is the activation of the obtained char, which can be physical or chemical (Yuen and Hameed, 2009). Physical activation consists of partially gasifying the char at a higher temperature (800–1000 °C) with oxidizing gases such as air, steam, carbon dioxide, or their mixtures to produce activated carbons with accessible internal porosity (Yuen and Hameed, 2009; Rashidi and Yusup, 2017). Chemical activation involves the impregnation of the precursor or char with chemical compounds (dehydrating and oxidizing agents) before or after the carbonization, respectively; either to dehydrate the precursor and promote the formation of a crosslinked structure or to remove the tar present inside the char pores (Danish and Ahmad, 2018; Yahya et al., 2015). Chemical activation has more advantages than physical activation including low activation temperature, shorter activation time, higher carbon yield, and incorporation of surface functional groups; it also generates greater porosity and surface area in the activated carbon (Danish and Ahmad, 2018; Maciá-Agulló et al., 2004).

The sequence of carbonization, physical and chemical activation offers different alternatives for the preparation of the activated carbon, thus resulting in adsorbents with different physicochemical characteristics. Activated carbons produced by carbonization and physical activation in one step may not have satisfactory performance to be used as adsorbents (Ioannidou and Zabaniotou, 2007). Meanwhile, activated carbons obtained by chemical activation before or after carbonization can have a high surface area, narrow micropore distribution, and high adsorption capacity (Gil et al., 2014); likewise, the chemical activation of the precursor, followed by carbonization and physical activation in a single step, allows to get activated carbons with better adsorption properties (Aguayo-Villarreal et al., 2017a; Lee et al., 2014). However, the preparation of activated carbons with selective adsorption capacity towards a specific compound is still a challenge; because the selectivity depends on the surface physical characteristics and its chemical composition; the tailoring of these surface characteristics is a difficult task.

In this study, the procedures for manufacturing low-cost activated carbons to separate benzene and cyclohexane are presented. The activated carbons were prepared from the coconut shell (Cocos nucifera) varying the type and concentration of the chemical agent, ratio mass of the precursor/volume of chemical agent, and time of physical activation using a Taguchi experimental design to evaluate their effect in the adsorption capacity. Acetic acid, zinc chloride and phosphoric acid were used in the chemical activation. The physicochemical characterization of activated carbons was performed using SEM/EDS, X-ray diffraction, FTIR, Boehm titration, determination of the zero-charge point and nitrogen adsorption. A lab-made dynamic system coupled to a GC-FID was used for the determination of the activated carbon adsorption capacity. After data analysis of the Taguchi experimental design, the best preparation conditions to obtain an activated carbon with the highest benzene adsorption capacity were established.

Table 1
Taguchi experimental design L_9 used in the preparation of activated carbons for benzene adsorption.

Activated carbon	Factor A: Chemical agent	Factor B: Concentration of chemical agent (M)	Factor C: Ratio (mass precursor/vol chemical agent)	Factor D: Physical activation time (h) with CO_2 at 800 °C (h)
E1	CH_3COOH	1.0	1:2	2.0
E2	CH_3COOH	0.5	1:1	1.0
E3	CH_3COOH	0.1	1:0.5	0.5
E4	$ZnCl_2$	1.0	1:1	0.5
E5	$ZnCl_2$	0.5	1:0.5	2.0
E6	$ZnCl_2$	0.1	1:2	1.0
E7	H_3PO_4	1.0	1:0.5	1.0
E8	H_3PO_4	0.5	1:2	0.5
E9	H_3PO_4	0.1	1:1	2.0

2. Materials and methods

2.1. Materials

All chemicals used in this study were reactive grade. Acetic acid (JT Baker), Benzene (99.0–99.5%, Sigma-Aldrich), carbon dioxide, cyclohexane (99.0–99.5%, Sigma-Aldrich), hydrochloric acid (JT Baker), deionized water, nitrogen, phosphoric acid (Jalmek), sodium bicarbonate (Fermont), sodium carbonate (Jalmek), sodium hydroxide (Sigma-Aldrich), and zinc chloride (JT Baker) were employed. The coconut shells (Cocos nucifera) were obtained from organic waste generated in local food industries.

2.2. Activated carbons

2.2.1. Pretreatment of the coconut shell

The coconut shell was ground and sieved to a particle size of 1 ± 0.1 mm. The grounded coconut shell was washed with deionized water at 25 °C until obtaining a constant pH value of the washing solution. Subsequently, it was dried at 70 °C for 24 h and stored for later use.

2.2.2. Preparation of activated carbons

The preparation of activated carbons consisted of two stages. In the first stage, the chemical activation of the precursor was carried out. For this, the grounded coconut shell was mixed with the chemical agent in a batch system, according to Table 1. This mixture was heated up to 100 °C until the solvent evaporated; then, the impregnated coconut shell was maintained at 70 °C for 24 h. In the second stage, both the pyrolysis of the precursor (800 °C, N_2 atmosphere) and its physical activation (800 °C, CO_2 atmosphere) was assessed. For this, 30 g of impregnated coconut shell (dry) were loaded in the quartz reactor of a horizontal tubular furnace Carbolite Eurotherm model CTF 12165/550. The pyrolysis was performed with N_2 atmosphere applying a segmented temperature gradient: initially, the temperature increased from 25 to 70 °C (at 5 °C/min rate and 1 h hold) and then increased to 800 °C (at 5 °C/min and maintained for 4 h). Subsequently, the physical activation was performed with CO_2 atmosphere for the time indicated in Table 1. Finally, nine activated carbons were obtained, which were washed with deionized water, dried, and stored for subsequent experiments.

2.2.3. Taguchi experimental design

The preparation of nine activated carbons was performed according to a Taguchi experimental design employing an orthogonal array type L_9, see Table 1. The factors evaluated were the type and concentration of the chemical agent, ratio mass of the precursor/volume of chemical agent, and the physical activation time with CO_2 at 800 °C. The response variable was the benzene adsorption capacity during the mixture separation. This experimental design was established with the aim to identify the best preparation conditions to obtain an optimized activated carbon with the highest benzene adsorption capacity.

2.2.4. Preparation of the activated carbon with the best benzene adsorption properties

Statistical data analysis of the Taguchi experimental design was used to identify the best preparation conditions to obtain the QB activated carbon with the highest benzene adsorption capacity during the separation of the binary mixture.

2.3. Physicochemical characterization of activated carbons

2.3.1. Fourier Transform-Infrared Spectroscopy (FT-IR)

Functional groups present on the surface of activated carbons were identified using a Thermo Scientific Nicolet-iS10 FT-IR spectrometer equipped with a deuterated triglycine sulfate detector (DTGS-KBr). Spectra were collected in the 4000–500 cm^{-1} spectral range. For sample preparation, the activated carbon was mixed with potassium bromide (KBr) at a weight ratio of 1:300 (g adsorbent/g KBr) using an agate mortar. The resulting powder mixture was compacted using a manual hydraulic press, and the pellets were used for the analysis.

2.3.2. Boehm titration

The acidic and basic functional groups present on the surfaces of activated carbons were quantified by the Boehm titration method (Boehm, 2002). Aqueous solutions of NaOH, Na_2CO_3, $NaHCO_3$, and HCl were prepared and used as reaction solutions. The concentration of each solution was 0.01 M. Three samples were prepared with each reaction solution for each activated carbon as follows: in a 50 mL Falcom tube, 20 mg of activated carbon and a given volume of the reaction solution were added. In the case of the NaOH, $NaHCO_3$ and HCl solutions, 20 mL were used for each sample; in the case of the Na_2CO_3 solution, 10 mL were used. These samples were kept under stirring for 24 h at 100 rpm and 30 °C. After 24 h, the solution was separated by decantation, and the amount used as aliquot in the titrations was 10 mL for the NaOH, $NaHCO_3$ and HCl solutions, and 5 mL for the Na_2CO_3 solution, to keep the same equivalence of the base. The titration was carried out using a 0.01 M HCl or NaOH solution until obtaining a pH of 7. The quantity of surface functional groups was calculated from the difference between the moles of acid or base initially available in the reaction solution and the moles of acid or base remaining in solution after the reaction. Eq. (1) was applied.

$$n_x = C_{Sr}V_{Sr} - C_{St}V_{St}\frac{V_{Sr}}{V_a} \tag{1}$$

Where n is the moles of functional groups on the surface of the activated carbon that reacted with the reaction solution during the mixing step, and x refers to the solutions of NaOH, Na_2CO_3, $NaHCO_3$, and HCl. The parameters C_{Sr} and V_{Sr} are the concentration and volume of the reaction solution mixed with the activated carbon. V_a is the volume of the aliquot taken from V_{Sr} for titration after the reaction. C_{St} and V_{St} are the concentration and volume of the titrant solution added to the aliquot analyzed.

The quantity of the different surface functional groups (phenolic, lactonic, and carboxylic groups) was calculated through the difference between the calculated amounts of reacted superficial functionality (n_x). NaOH solution neutralizes the phenolic, lactonic, and carboxylic groups, giving the total quantity of surface acidic groups; Na_2CO_3 solution reacts with carboxyl and lactonic groups; while $NaHCO_3$ solution neutralizes only the carboxylic acid groups. Thus, the difference between nNaOH and $n$$Na_2CO_3$ gives the total number of phenol groups, and the difference between $n$$Na_2CO_3$ and $n$$NaHCO_3$ provides the total number of lactonic groups, and $n$$NaHCO_3$ corresponds to the total number of carboxylic acid groups (Goertzen et al., 2010; Seung Kim and Rae Park, 2016), while nHCl indicates the quantity of total basic groups on the adsorbent surface.

2.3.3. pH of point of zero charge (PZC)

The PZC of the activated carbons was determined through the pH drift method using a potentiometer Orion 3 Start pH Benchtop Thermo Scientific. HCl or NaOH solution was used to adjust pH value of stock solutions at 2, 4, 6, 8, 10 and 12. The pH of these solutions was registered as pHinitial. Activated carbon samples (20 mg) were placed into 20 mL of stock solution with different pH (2, 4, 6, 8, 10, and 12) in a 50 mL Falcom tube; then, these samples were shaken for 24 h at 100 rpm and 30 °C. After 24 h, the activated carbon was separated from the solution by decantation; the final solution pH was measured and registered as pHfinal. Finally, the pHinitial *versus* the pHfinal was plotted and the first point where the curves intersected (pHinitial = pHfinal) was taken as the PZC.

2.3.4. X-ray powder diffraction (XRPD)

The X-ray powder diffraction patterns of all activated carbons were obtained at ambient temperature using a PANalytical X'Pert PRO diffractometer equipped with a CuK_α X-ray source operated at 45 kV and 40 mA where a 10 mm fixed mask, a collimator slit of 1/2° and an anti-scatter slit of 1/4° were used at primary beam. For sample preparation, each activated carbon was pulverized using an agate mortar, and the resulting powder was used for the analysis. The peaks associated to the crystalline phases in the diffraction patterns were identified using X'Pert HighScore Plus software.

2.3.5. Scanning electron microscope analysis

The morphology of the activated carbons was analyzed using a scanning electron microscope (SEM/EDS) TM3000 Hitachi Tabletop Microscope with an acceleration voltage of 20 kV.

2.3.6. Nitrogen adsorption

Textural parameters of activated carbons were obtained from the nitrogen adsorption/desorption isotherms, which were determined at 77 K using a Micromeritics ASAP 2020 porosimeter. The specific surface area, microporous surface area, external surface area, pore volume, and micropore volume of the activated carbons were determined employing the Langmuir, Dubinin–Radushkevich, and t-plot models. Likewise, the pore size width of each adsorbent was determined using the Horvath-Kawazoe model.

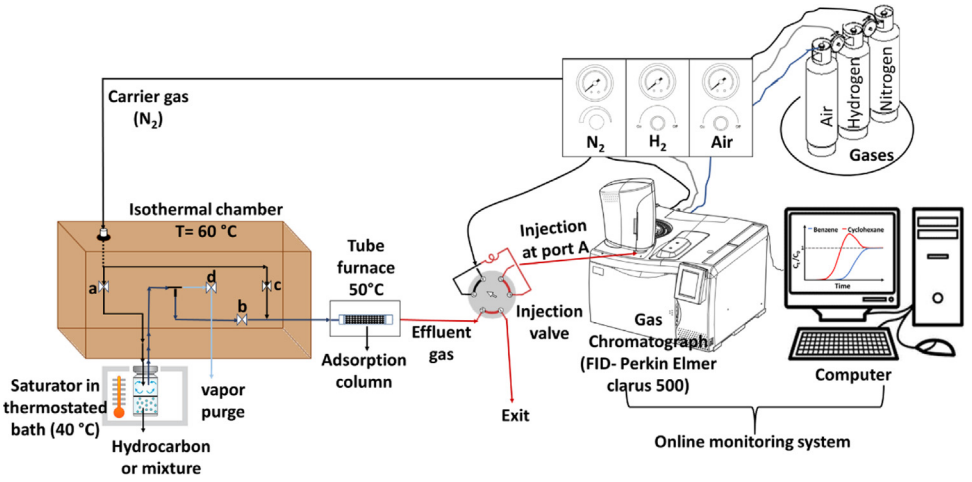

Fig. 1. Schematic diagram of the set up utilized in fixed-bed adsorption experiments.

2.4. Chromatographic analyses and calibration curves

Sample analyses were carried out using a Perkin Elmer Gas chromatograph (GC), model Clarus 500, coupled to a flame ionization detector (FID). A capillary column SPB-624 (60 m × 0.25 mm internal diameter × 0.14 μm film thickness) from Supelco (Merck, Guadalajara, Mexico) was used. Nitrogen was employed as carrier gas set at 30 psi. GC oven temperature was isothermally programmed at 100 °C. The temperatures of the injector and detector ports were kept at 150 and 220 °C, respectively. The injector was operated in a split mode using a nitrogen flow-rate of 8 mL/min.

Calibration curves to quantify cyclohexane and benzene concentration in the effluent gas stream were obtained as follows: both cyclohexane and benzene were prepared at 5, 10, 20, 40, 60, 80, and 100 mM using hexane as solvent. One microliter of these solutions was injected into the GC-FID and peaks area was recorded, considering the retention times of both analytes (cyclohexane: 7.96 min and benzene: 8.37 min). The calibration equation that describes a straight line was obtained via plotting each hydrocarbon area (*y-axis*) *versus* the concentration of each injected dissolution (*x-axis*). In all cases, the intercepts were not significantly different from zero. The linear regression coefficient for benzene and cyclohexane was 0.9996 and 0.9992, respectively.

2.5. Fixed-bed adsorption experiments

Fixed-bed adsorption experiments were carried out using the system shown in Fig. 1, which was assembled in the laboratory and was composed of a gas saturator, an isothermal chamber, a tube furnace, an automatic injection valve, and a steel adsorption column (3.3 cm long × 5 mm internal diameter × 0.5 mm thickness). It was coupled to a GC system with a flame ionization detector (GC-FID). The experiments were performed at 50 °C under monocomponent and binary gas conditions. Benzene and cyclohexane were used as adsorbates. Adsorbate volume used was 3 mL for both the monocomponent and binary analysis, but the mixture was prepared with the same amount by weight of each hydrocarbon. Nitrogen was used as carrier gas at a flow-rate of 5.5 mL/min. In each experiment, the hydrocarbons vapors were generated in a saturator maintained at 40 °C; these vapors were purged for 15 min leaving only valves "a" and "d" opened, to guarantee that the hydrocarbons concentration at the entrance of the adsorption column remained constant during the experiment. The adsorption process was started leaving only valves "a" and "b" opened; so that the nitrogen passed through the saturator and carried the hydrocarbon vapors towards the adsorption column packed with 0.3 g of activated carbon and maintained at 50 °C. The gas flow at the adsorption column exit (effluent gas) was directed to the automatic injection valve to inject 20 μL to the GC-FID; the injections were programmed with an interval of two minutes. When the activated carbon became saturated with adsorbate, the adsorption column was heated at 200 °C with N_2 flow to remove the adsorbate (valve "c" opened, valves "a", "b", and "d" closed). GC-FID equipment allowed both quantifying the adsorbate in the effluent gas and monitoring the adsorption/desorption process online.

Each adsorption experiment was stopped when the adsorbates concentration of the effluent gas matched the adsorbate concentration of the inlet flow and remained constant for 30 min. The experiments were carried out by triplicate and the values corresponding to carrier gas flow rate (Q, L/min), activated carbon weight (w, g), time (t, min), and adsorbate concentration of the flow at the inlet and outlet of the adsorption column (C_o and C_t, mmol/L), were recorded. Breakthrough curves were obtained by plotting C_t/C_o *versus* time, and the adsorption capacity (q_t, mmol/g) was obtained

by numerical integration of the breakthrough curves using the following Eq. (2) (Gil et al., 2014; Aguayo-Villarreal et al., 2017b):

$$q_t = \frac{QC_o}{w}\int_0^{t_s}(1-\frac{C_t}{C_o})dt \tag{2}$$

Where t_s is the saturation time (min) when $C_t = C_o$ at adsorption column exit. Considering that the mass transfer zone (MTZ) is the part of the packed bed where the adsorption mainly occurs and that the breakthrough curve describes its displacement along the packed bed during the adsorption process, the performance of each activated carbon bed was evaluated via two characteristic parameters of the MTZ, which were the fractional capacity (Ø) and the length of the mass transfer zone (H_{MTZ}). The breakthrough curves were also used to calculate these parameters using the following equations (Gil et al., 2014; Aguayo-Villarreal et al., 2017b).

$$Ø = \frac{\int_{t_b}^{t_s}(C_o - C_t)dt}{(t_s - t_b)\,C_o} \tag{3}$$

$$H_{MTZ} = \frac{L*(t_s - t_b)}{t_s + (t_s - t_b)Ø} \tag{4}$$

Where C_o and C_t correspond to the adsorbate concentration of the flow at the inlet and outlet of the adsorption column (mmol/L), t_b is the breakthrough time when $C_t/C_o = 0.05$, t_s is the saturation time when $C_t/C_o = 1$, L is the length of the bed (cm), and Ø is the fractional capacity.

2.6. Statistical analysis of the Taguchi experimental design

The statistical analysis of the Taguchi experimental design was carried out using as response variable the benzene adsorption capacity during the separation of the cyclohexane/benzene mixture. This analysis was performed to determine the factors of the preparation process that have the greatest influence on this variable and the corresponding preparation conditions that allow to improve its value. For this purpose, the analysis of experimental design results was done using the signal/noise ratio (S/N) applying the approach of the "larger the better" to improve the benzene adsorption properties of activated carbons. The S/N ratio was calculated from Eq. (5) (Elizalde-González and Hernández-Montoya, 2009).

$$\frac{S}{N} = -10\log\frac{\sum_i(1/{q_i}^2)}{n} \tag{5}$$

Where q_i is the benzene adsorption capacity during the separation of the cyclohexane/benzene mixture of each activated carbon and n is the number of replicates of the adsorption experiment. An analysis of variance (ANOVA) was carried out to determine the factors that have the greatest influence on the response variable.

3. Results and discussion

3.1. Physicochemical characterization of activated carbons

3.1.1. Fourier Transform-Infrared Spectroscopy (FT-IR)

FT-IR spectra of the activated carbons from coconut shell are shown in Fig. 2. All activated carbons exhibited similar spectra thus suggesting they had similar functional groups but at different concentrations because their spectra intensity varied slightly from one activated carbon to another. According to Fig. 2, the absorption bands at around 3700 and 3400 cm^{-1} were assigned to the stretching vibration of hydroxyl groups (O-H) from carboxyls, phenols, alcohols, and adsorbed water (Mohammed et al., 2015). The bands at 2920 and 2850 cm^{-1} were attributed to the symmetric (2850 cm^{-1}) and asymmetric (2920 cm^{-1}) stretching vibration of the C-H bond of aliphatic (-CH_3, -CH_2, -CH) compounds (Long et al., 2018; Saka, 2012). The small band at 1730 cm^{-1} was due to the stretching vibration of the C=O bond of carbonyl/carboxyl groups (Saka, 2012). The band observed at 1560 cm^{-1} was assigned to the stretching vibration of the –C=C and C=C bonds of alkenes present in the aromatic skeleton of lignin (Mohammed et al., 2015). The small band at 1430 cm^{-1} was attributed to either O-H bond bending vibration in carboxyl groups or C–H bending vibrations in CH_2 or CH_3 groups (Wang et al., 2015b; Foo and Hameed, 2012). The band located at 1046 cm^{-1} corresponded to both C–O bond stretching vibration in primary alcohols and O-H bond bending vibration in phenolic groups (Kumarasinghe et al., 2019; Zhao et al., 2018).

3.1.2. Boehm titration

The concentration of the acidic and basic surface groups and the PZC of the activated carbons are shown in Table 2. It was observed that the concentration of the surface functional groups varied from one activated carbon to another due to their preparation conditions. The different physical and chemical modifications of the precursor impacted on the surface chemistry due to the incorporation of different heteroatoms (oxygen, hydrogen, phosphorus) at the edges of graphite-like lays, thus forming organic functional groups such as carboxylic acids, lactones, phenols, carbonyls, aldehydes, ethers,

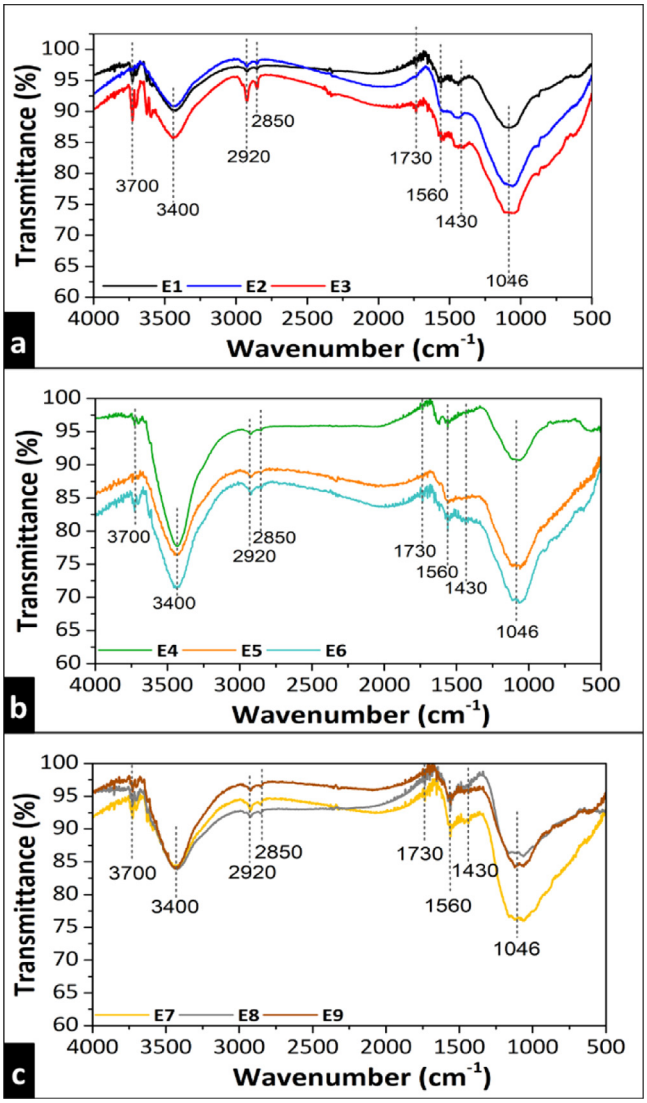

Fig. 2. FT-IR spectra of activated carbons prepared from coconut shell. Activation agent: (a) CH_3COOH, (b) $ZnCl_2$, (c) H_3PO_4.

and other phosphate-containing groups. Note that these functional groups determine the moisture content, catalytic properties, acid/base character and adsorption capacity of the activated carbons (Li, 2012; Salame and Bandosz, 2001). Results indicated that each activated carbon showed a unique surface chemistry that determined its interaction with adsorbates.

It was also observed that the acidic groups corresponding to carboxylic and phenolic groups were predominant on the surface of most of activated carbon samples. Besides, it was noted that the samples E3, E6, E7, E8, and E9 presented a high total content of acids groups, which provided hydrophilic sites on their surface that favored the cation exchange and the interaction with polar adsorbates (Boehm, 1994). According to this result, the development of acidic surface groups was higher in these materials (E8>E7>E6>E9); because the chemical treatment contributed to the generation of unsaturated sites, in which a greater quantity of oxygen was chemisorbed during physical activation with CO_2. However, sample E9 displayed a lower content of acid groups than samples E7 and E8 because its physical activation time at 800 °C was longer (E7: 5 h, E8: 4.5 h, and E9: 6 h). This preparation condition contributed to the decomposition of the acidic functional groups in CO and CO_2, at the same time that favored the formation of basic superficial groups (Boehm, 1994; Prahas et al., 2008; Hadi et al., 2015; Shen et al., 2010). Samples E1, E2, E4, and E5 exhibited a basic surface character due to their high total content of basic groups, the intrinsic mineral salts of the precursor and the high π-electron density at the surface graphene layers (Radovic et al., 1996). Note that the basic surface groups provide surface hydrophobicity and promote the anion exchange and the interaction with non-polar adsorbates (Boehm, 1994; Shen et al., 2010; Radovic et al., 1996, 1997). The type of activating agent and the conditions of carbonization/physical activation favored the development of

Table 2
Surface functional groups and PZC of activated carbons prepared from coconut shell.

Functional groups	Concentration (mmol/g)								
	E1	E2	E3	E4	E5	E6	E7	E8	E9
Carboxylic acids	0.061	0.067	0.081	0.481	0.155	1.442	1.526	2.331	0.971
Lactonic	0.086	0.065	0.016	–	–	–	–	–	–
Phenolic	0.029	–	–	0.108	0.027	0.070	1.390	1.329	0.347
Total acidic groups	0.176	0.132	0.097	0.589	0.182	1.512	2.917	3.660	1.318
Total basic groups	0.290	0.740	0.021	0.678	0.893	0.731	–	0.015	0.317
PZC	6.9	6.8	7.0	6.3	7.0	6.9	3.8	2.0	6.5

a basic surface in those materials. Activated carbon E2 showed a higher content of basic groups and a lower content of acidic groups than sample E1. This finding suggested that possibly the chemical treatment with acetic acid (E1: 1M, E2: 0.5M) did not cause the complete elimination of the intrinsic mineral salts of the coconut shell, such as calcium carbonate, which was abundant in this precursor (Raveendran et al., 1995; Afrane and Achaw, 2008; Liyanage and Pieris, 2015). In the case of sample E2, the heat treatment favored the calcium carbonate precipitation on the carbon surface thus increasing its basic character. In the case of sample E1, the chemical treatment was more intense due to the high concentration of the chemical agent, so a greater elimination of these salts was possible.

In the case of samples E4 and E5 that were chemically activated with $ZnCl_2$, the heat treatment contributed to the development of zinc oxide on their surface, thus increasing their surface basicity. The heating during the chemical activation led to the generation of zinc hydroxide on the surface of the precursor ($ZnCl_2 + 2H_2O \rightarrow Zn(OH)_2 + 2HCl$). Then, the zinc hydroxide decomposed into zinc oxide ($Zn(OH)_2 \rightarrow ZnO + H_2O$) during the carbonization of the impregnated precursor at 800 °C. However, the development of basic groups was higher in sample E5 since its carbonization/physical activation time at 800 °C was longer than samples E4 and E6 (E4: 4.5 h, E5: 6 h, and E6: 5 h).

The surface acidic groups, especially lactonic and carboxylic groups, increased when acetic acid was the chemical agent (Long et al., 2018). It was expected that activated carbons E1, E2, and E3 showed a higher content of carboxylic acids on their surface compared to the other materials, and that the amount of these groups would increase with the increment of CH_3COOH concentration in the preparation of these adsorbents. However, the results indicated that they did not present a significant content of phenolic groups and were the only ones that presented lactonic groups on their surface. According to Long et al. (2018), lactonic groups were formed due to the reaction between carboxyl groups and phenolic hydroxyl groups during the carbonization/activation of the precursor at high temperatures (500–600 °C), which caused the decrease of carboxyl groups and phenolic hydroxyl groups on the surface of activated carbons.

3.1.3. PZC

Results of Table 2 indicated that most of the activated carbons presented a PZC between 6 and 7, except for samples E7 and E8 where their PZC was 3.8 and 2, respectively. PZC is the pH at which the adsorbent surface has no electrical charge (Nasiruddin Khan and Sarwar, 2007). In this sense, if the adsorbent is immersed into an aqueous solution with a pH < PZC, its basic surface groups will be dissociated producing a positive charge and favoring anion exchange processes. In contrast, if solution pH > PZC of activated carbon, its surface will present a negative charge caused by the dissociation of the acidic surface groups and will favor cation exchange processes.

3.1.4. XRPD

The X-ray diffraction patterns of the activated carbons from coconut shell are shown in Fig. 3-a. The peak at $2\theta = 44.6°$ observed in all diffractograms was attributed to the (101) plane corresponding to graphite (00-001-0646) and this peak was the only observed in the diffraction patterns of samples E7, E8, and E9. A weak peak was also observed at $2\theta = 29.40°$ in the diffractograms of samples E1, E2, and E3, which was attributed to the (104) plane of calcium carbonate ($CaCO_3$, 00-005-0586). Other characteristic peaks were also registered at $2\theta = 31.69°$, 34.38°, 36.18°, 47.45°, and 56.46° in the diffraction patterns of samples E4, E5, and E6, which were attributed to the crystal planes (100), (002), (101), (102), and (110) of the zinc oxide (ZnO, 01-079-0207). Unlike the other materials, the diffractogram of activated carbon E4 also showed a weak peak at $2\theta = 26.4°$ attributed to the (002) plane of graphite (00-001-0646). ZnO and $CaCO_3$ were possibly generated during the thermal processes as a product of secondary chemical reactions between the raw material components and activation agents or due to the residual mineral content intrinsically present in the precursor (Ramirez-Gutierrez et al., 2020; Hong et al., 2019; Shin et al., 2011). This result confirmed the findings from Boehm titration about the surface character of samples E1, E2, E4, and E5.

3.1.5. SEM analysis

SEM micrographs at 500x are shown in Fig. 3-b. It was observed that all activated carbons exhibited a heterogeneous surface morphology, which was composed of grouped flakes in an irregular form. Small white particles with no specific shape corresponding to zinc oxide (confirmed with the XRPD analysis) were observed on the surface of carbons activated obtained with $ZnCl_2$ (E4, E5, and E6). Also, EDS analysis revealed the presence of carbon (C), oxygen (O) and zinc (Zn)

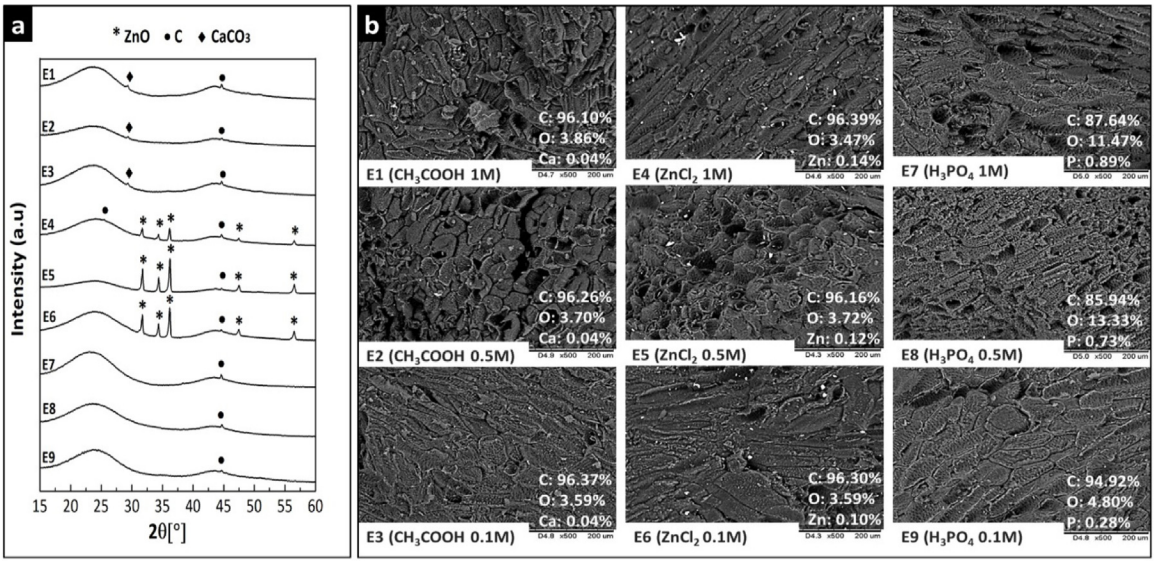

Fig. 3. (a) XRD patterns, (b) SEM micrographs (500x) and EDS analysis results of activated carbons obtained from coconut shell.

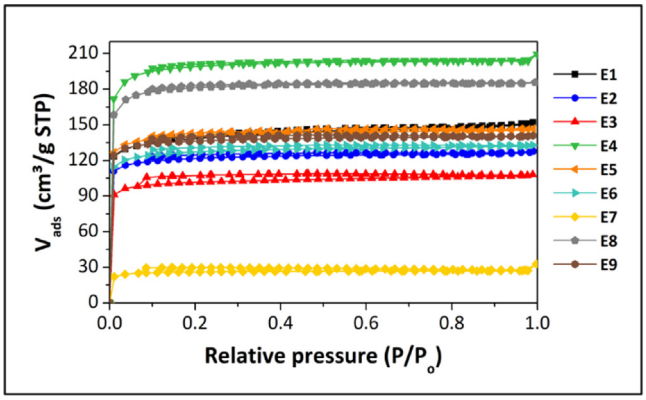

Fig. 4. Nitrogen adsorption–desorption isotherms of activated carbons obtained from coconut shell.

dispersed throughout the surface, thus confirming the dispersion of ZnO particles on the surface of these adsorbents. Likewise, EDS analysis indicated the presence of calcium (Ca) in the carbons activated with CH_3COOH (E1, E2, and E3) and phosphorus (P) in the carbons activated with H_3PO_4 (E7, E8, and E9). EDS analysis also showed the presence of carbon and oxygen in all the samples.

3.1.6. Textural parameters

Nitrogen adsorption/desorption isotherms of activated carbons are shown in Fig. 4. According to the IUPAC classification, all the isotherms corresponded to the type I isotherm (Langmuir type isotherm), which is characteristic of microporous adsorbents with small external surfaces where the micropore filling may take place at low relative pressure (P/Po). It was also observed that the isotherms exhibited a small H4 type hysteresis loop, that was indicative of the low volume of mesopores in the analyzed activated carbons (Zhao et al., 2018; Thommes et al., 2015), which was also characteristic of slit-shaped pores (Prahas et al., 2008; Puziy et al., 2005).

The surface physical characteristics of the activated carbons were obtained by means of different models (Table 3). Samples E4 (894.05 m^2/g), E8 (808.04 m^2/g), E1 (658.31 m^2/g), E5 (637.47 m^2/g) and E9 (612.68 m^2/g) showed the highest surface area calculated with Langmuir model. Calculations with the Dubinin–Radushkevich model indicated that samples E4, E8, E5, E9, and E1 showed a high microporous surface area (884.27, 805.66, 613.74, 597.66, and 594.62 m^2/g, respectively), and a high total volume of pores (V_{Tp}) and micropores (V_{mi-DR}) where the tendency of the percentage of micropores was: E8 (99.56%)>E9 (97.49%)>E4 (96.94%)>E5 (96.04%). Besides, it was observed that all activated carbons exhibited a small external surface (A_{Sext}) compared to their total and microporous surface area, and mean pore width values (W_{HK}) less than 20 Å.

Table 3
Surface physical characteristics of activated carbons obtained from coconut shell.

Surface parameter	E1	E2	E3	E4	E5	E6	E7	E8	E9
Langmuir									
A_S (m^2/g)	658.31	551.90	469.68	894.05	637.47	578.15	121.20	808.04	612.68
R^2	1.00	1.00	1.00	1.00	1.00	1.00	1.00	1.00	1.00
Dubinin–Radushkevich (DR)									
A_{SDR} (m^2/g)	594.62	571.83	445.71	884.27	613.74	554.92	116.15	805.66	597.66
R^2	1.00	1.00	1.00	1.00	1.00	1.00	1.00	1.00	1.00
t-plot									
A_{Sext} (m^2/g)	81.71	42.34	37.35	69.89	54.73	45.35	10.10	57.54	42.23
R^2	1.00	0.99	0.98	0.98	0.99	0.99	0.97	0.98	0.99
Mean pore width									
W_{HK} (Å)	10.28	10.23	10.30	10.21	10.24	10.21	10.38	10.22	10.19
Pore volume									
V_{Tp} (cm^3/g)	0.24	0.20	0.17	0.32	0.23	0.21	0.05	0.29	0.22
$V_{mi-tplot}$ (cm^3/g)	0.18	0.17	0.14	0.28	0.19	0.18	0.04	0.25	0.19
V_{mi-DR} (cm^3/g)	0.21	0.19	0.16	0.31	0.22	0.20	0.04	0.29	0.21
V_{me} (cm^3/g)	0.024	0.010	0.009	0.010	0.009	0.008	0.010	0.001	0.005
% micropores	89.79	95.09	94.74	96.94	96.04	95.90	81.20	99.56	97.49
% mesopores	10.21	4.91	5.26	3.06	3.96	4.10	18.80	0.44	2.51

A_S: total surface area, A_{SDR}: microporous surface area, A_{sext}: external surface area (pore free), V_{Tp}: total pore volume, V_{mi}: total volume of micropores; V_{me}: total volume of mesopores ($V_{me} = V_{Tp}–V_{mi}$); W_{HK}: mean pore width obtained with Horvath–Kawazoe (HK) model.

A trend was observed of the surface area, microporous surface area, external surface area, total pore volume, micropores, and mesopores in the activated carbons with a high concentration of CH_3COOH (E1> E2> E3) and $ZnCl_2$ (E4> E5> E6); this can be explained considering that the chemical agent promoted the dehydration, degradation, and solubilization of the components of the raw precursor. In addition, the chemical agent caused the formation of cross-links between lignocellulosic compounds, which served as a template for the development of porosity during the pyrolysis of the impregnated precursor. In this sense, the formation of this cross-linking was higher when the concentration of the activating agent increased from 0.1 to 1 M. This finding agreed with the results by Long et al. (2018). These authors observed that the values of surface characteristics increased as the concentration of the acetic acid solution increased from 1 to 2 M. In another study, He et al. (2013) reported that the surface area and volume of pores, micropores, and mesopores increased as the mass ratio $ZnCl_2$/precursor increased, thus suggesting that the $ZnCl_2$ acted as a dehydration agent and template during the activation process, which leaded to the charring and aromatization of the carbon skeleton, and therefore, the creation of porosity.

In the case of activated carbons obtained with H_3PO_4, sample E8 showed surface area, microporous surface area, external surface area, pore volume, and micropores higher than those of samples E7 and E9. According to Nieto-Delgado and Rangel-Mendez (2011), the surface area of the activated carbon increased with H_3PO_4 concentration until a maximum value; after that maximum value, the surface area decreased with increments of concentration of the chemical agent to values higher than 2.5 g H_3PO_4/g precursor. Puziy et al. (2005) also reported that in the activated carbons obtained from lignocellulosic precursors chemically treated with H_3PO_4, the reduction of pore volume and surface area could be attributed to contraction of the material caused by prolonged exposure to high temperatures (400–800 °C) during the carbonization/activation. According to these authors, the phosphate and polyphosphate bridges formed during pyrolysis by the interaction between the phosphoric acid and the lignocellulosic polymers of the precursor, become thermally unstable above 450 °C, leading to contraction of the structure of activated carbons, and therefore, to the decrease of porosity.

It was also observed that the development of mesopores was greater in samples E1 and E7, which were chemically activated with a 1 M solution of acetic acid and phosphoric acid and physically activated for two and one hours, respectively (Table 1). This finding indicated that the conditions of physical activation (time and temperature) with CO_2 favored the opening and widening of the micropores created by the chemical treatment in these adsorbents, causing the increment of their mesoporosity.

3.2. Fixed-bed adsorption measurements

3.2.1. Single adsorption of benzene and cyclohexane

Fig. 5 shows the breakthrough curves for the adsorption of benzene and cyclohexane for the nine activated carbons and the calculated values q_t, Ø and H_{MTZ} are reported in Table 4.

Activated carbons E1, E4, E5, and E8 showed a longer breakthrough time (i.e., time at $C_t/C_o = 0.05$) and, consequently, a higher adsorption capacity for both cyclohexane (E4>E8>E1>E5) and benzene (E4>E1>E8>E5). It was also observed that the breakthrough times for benzene adsorption were higher than those for cyclohexane, indicating that these activated carbons presented a higher capacity to adsorb benzene. The packed beds with adsorbents E1, E4, E5, E8, and E9 registered

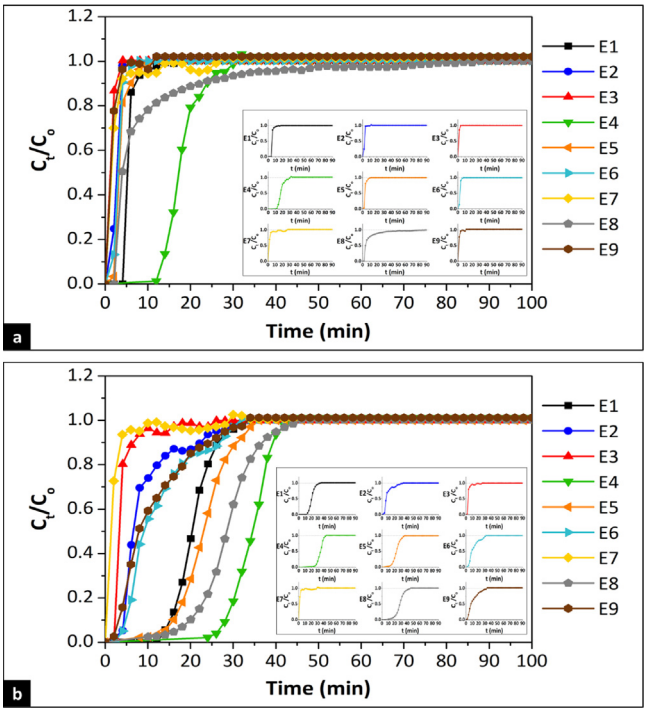

Fig. 5. Breakthrough curves for the adsorption of (a) cyclohexane and (b) benzene using activated carbons prepared from coconut shell.

Table 4
Parameters of breakthrough curves of the adsorption of cyclohexane and benzene using activated carbons prepared from coconut shell.

Activated carbon	Activating agent and concentration	Cyclohexane			Benzene		
		q_t (mmol/g)	Ø	H_{MTZ} (cm)	q_t (mmol/g)	Ø	H_{MTZ} (cm)
E1	CH_3COOH, 1 M	8.41	0.11	2.34	33.95	0.31	1.70
E2	CH_3COOH, 0.5 M	3.59	0.23	2.58	13.48	0.19	2.47
E3	CH_3COOH, 0.1 M	1.78	0.30	2.47	6.12	0.09	2.79
E4	$ZnCl_2$, 1 M	25.20	0.31	1.62	51.40	0.44	1.12
E5	$ZnCl_2$, 0.5 M	4.72	0.16	2.41	32.44	0.42	1.62
E6	$ZnCl_2$, 0.1 M	4.14	0.31	2.32	17.82	0.28	2.31
E7	H_3PO_4, 1 M	2.99	0.09	3.02	3.01	0.08	3.04
E8	H_3PO_4, 0.5 M	8.59	0.08	2.97	32.48	0.41	1.68
E9	H_3PO_4, 0.1 M	1.85	0.14	2.88	13.72	0.28	2.43

higher Ø values for the adsorption of benzene (E4>E5>E8>E1>E9) than for cyclohexane, which indicated that these beds presented a greater efficiency for adsorbing benzene in the mass transfer zone. Moreover, packed beds of activated carbons E2, E3, E6, and E7 presented higher Ø values in cyclohexane adsorption (E6>E3>E2>E7) than for benzene, being greater their efficiency to adsorb cyclohexane in the mass transfer zone. Packed beds of adsorbents E1, E2, E4, E5, E6, E8, and E9 showed lower H_{MTZ} values for benzene adsorption (E4<E5<E8<E1<E6<E9<E2) than for cyclohexane adsorption; this finding indicated that they presented less resistance to diffusion of the adsorbate. These results show that the activated carbons have different adsorption capacities, which makes sense because these materials were obtained under different preparation conditions. Thus, each activated carbon presents a unique surface physicochemical characteristics, which determined the interaction with the evaluated adsorbates.

According to Gil et al. (2014) and Gabelman (2017), the shape of the breakthrough curves can be related to the efficiency of the mass transfer from the gas phase to the adsorbent surface. Therefore, adsorbents with steep slope breakthrough curves can adsorb the adsorbate more easily and efficiently in the mass transfer zone, which agreed with the breakthrough curves of the activated carbons E1, E4, E5, and E8 (Fig. 5-b) that presented higher benzene adsorption capacity than that of cyclohexane and also registered the highest Ø values and lowest H_{MTZ} values. This result was promising for industrial applications because the operation of packed beds with minimum mass transfer resistances can guarantee the maximum use of the adsorbent during the dynamic adsorption process, which is advantageous from an operating and economic points of view.

Table 5
Results of the binary adsorption of the cyclohexane and benzene using activated carbons obtained from coconut shell.

Activated carbon	Cyclohexane					Benzene			S (q_{tb}/q_{tc})
	q_{tc} (mmol/g)	q_f (mmol/g)	q_d (mmol/g)	Ø	H_{MTZ} (cm)	q_{tb} (mmol/g)	Ø	H_{MTZ} (cm)	
E1	4.78	2.02	2.76	0.58	1.14	27.01	0.33	1.97	5.65
E2	1.84	1.57	0.27	0.64	1.71	9.79	0.15	2.75	5.32
E3	0.75	0.74	0.01	0.32	2.43	4.84	0.15	2.71	6.45
E4	12.83	5.45	7.38	0.55	0.97	32.36	0.43	1.93	2.52
E5	2.61	0.00	2.61	0.50	2.09	28.96	0.48	1.87	11.10
E6	1.95	1.76	0.19	0.62	1.72	14.64	0.28	2.49	7.51
E7	0.77	0.68	0.09	0.17	1.97	1.35	0.11	2.96	1.75
E8	4.63	3.64	0.99	0.29	2.15	25.07	0.45	1.96	5.41
E9	0.49	0.00	0.49	0.46	2.19	6.91	0.33	2.37	14.10

q_{tc}: total amount of cyclohexane initially adsorbed, q_f: amount of cyclohexane remaining in the adsorbent, q_d: amount of cyclohexane displaced to the effluent stream, q_{tb}: total amount of benzene adsorbed.

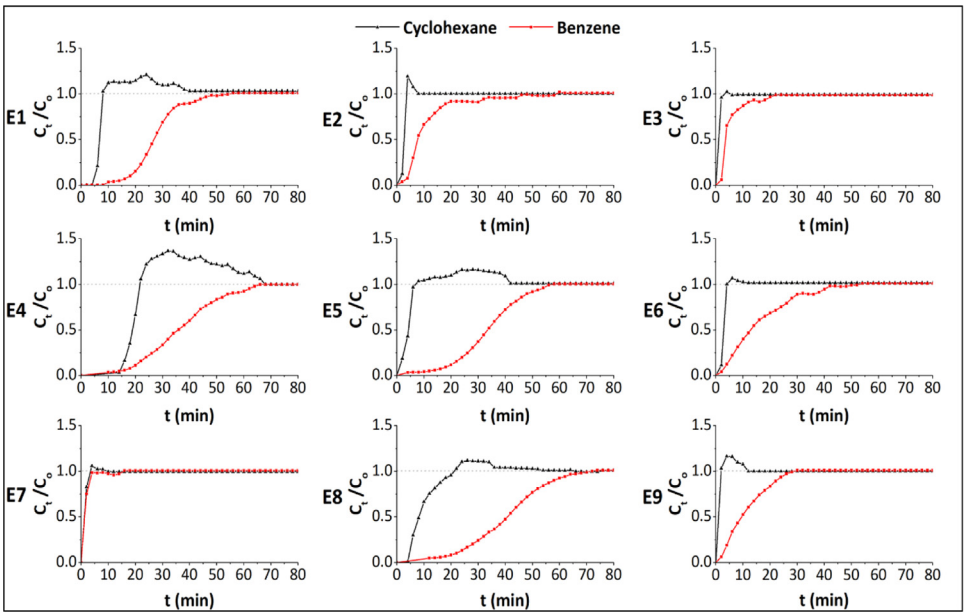

Fig. 6. Breakthrough curves for the binary adsorption of cyclohexane and benzene using activated carbons prepared from coconut shell.

3.2.2. Binary adsorption of benzene and cyclohexane

Calculated values of q_t, Ø, and H_{MTZ} for the binary adsorption of cyclohexane and benzene on tested activated carbons are summarized in Table 5 and the corresponding breakthrough curves are presented in Fig. 6. Activated carbon E4 showed the highest adsorption capacities for both hydrocarbons in the binary mixture. Although the benzene adsorption capacity of sample E4 was higher, its selectivity was lower than other activated carbons (E9>E5>E6>E3>E1>E8>E2>E4>E7). All activated carbons preferentially adsorbed benzene, but samples E1, E4, E5, and E8 showed the highest benzene adsorption capacity.

Results of Tables 4 and 5 indicated that the fractional capacity of the packed beds was greater in binary adsorption than in the monocomponent gas adsorption. This tred was due to the initial hydrocarbons concentration in the binary mixture was lower (C_o: 38.64 mmol/L) than in the monocomponent gas adsorption (C_o: 71.15 mmol/L), and the adsorption efficiency of packed beds increased when low adsorbate concentrations were used. Table 5 also indicated that the packed beds of activated carbons E1, E4, and E5 showed high Ø values and low H_{MTZ} values, confirming that these materials can adsorb the hydrocarbons more easily and efficiently in the mass transfer zone.

Fig. 6 shows that cyclohexane was the first breakthrough component at the outlet (effluent) and presented a roll-up effect, that is, the outlet concentration exceeded the inlet concentration ($C_t/C_o > 1$) as the activated carbon continued adsorbing benzene; when they reached the saturation of 90%–95% with benzene, the cyclohexane effluent concentration decreased and equaled to the inlet concentration. This result suggested that at the beginning of the binary adsorption, both hydrocarbons were adsorbed on the active sites of the activated carbons; when there were no more active sites available, the benzene molecules replaced the cyclohexane molecules previously adsorbed, scrolling them towards the outlet. Therefore, the cyclohexane roll-up effect in the binary mixture was due to a competitive adsorption of benzene.

According to the results shown in Table 5, adsorbents E1, E4, E5, and E9 showed the highest percentage of cyclohexane displacement (57.7%, 57.5%, 100%, and 100%, respectively). However, the activated carbons E5 and E9 were the only ones that achieved the separation of cyclohexane/benzene mixture. Although the adsorbent E9 showed a high selectivity, its benzene adsorption capacity was lower than the adsorbent E5.

These results agreed with those reported by other authors using different adsorbents and adsorbates. Sui et al. (2019), Maitlo et al. (2019), and Hernández-Hernández et al. (2017) observed the competitive effect during the adsorption of the acetone/ethyl acetate mixture on silica gels, the benzene/toluene adsorption on covalent organic polymers, and the separation of copper/zinc mixture on bone char, respectively.

It is important to note that the adsorbents E1, E4, E5, and E8 presented high adsorption capacities in both single and binary adsorption experiments (Tables 4 and 5). Based on the characterization results of activated carbons E4 and E5, the zinc oxide formed on adsorbent surface promoted a significant development of active sites that favored the interaction with the evaluated adsorbates. This was in concordance with other studies, which indicated that the incorporation of metallic oxides on the activated carbons surface improved their interaction with volatile organic compounds and increased their adsorption capacities.

Despite the high adsorption capacity of activated carbon E4, its selectivity towards benzene in the binary mixture separation was lower than that of the samples E5. Furthermore, the basic surface character of activated carbon E5 (24% higher than sample E4) contributed to its selective adsorption capacity. These basic functional groups provided hydrophobicity to the adsorbent surface (Boehm, 1994; Shen et al., 2010), favoring π-π dispersion interactions between benzene and the surface graphene layers of this adsorbent (Radovic et al., 1996, 1997). Instead, the surface of activated carbons with an acidic surface character, as the sample E4, had more hydrophilic sites (Boehm, 1994). This result confirmed that the high selectivity was more influenced by the nature of the surface functional groups of adsorbents rather than by their textural parameters such as the surface area and total pore volume.

Another important observation was that the samples E1 and E8 adsorbed 93.3% and 86.6% of benzene adsorbed by the sample E5 the in binary mixture (Table 5). Based on the preparation conditions and characterization results, the benzene adsorption capacity of activated carbons E1 and E8 may depend more on their surface physical characteristics than on their surface chemistry. In this sense, the activated carbon E1 exhibited a basic surface character; but registered a lower content of basic surface functional groups than the sample E5. By this reason, its adsorption capacity was not attributed only to its surface chemistry. The activated carbon E8 exhibited an acidic surface character and showed a higher total content of acid surface functional groups than the adsorbent E5. As stated, these surface functional groups favored the interaction with polar compounds, so its adsorption capacity was not attributed to its surface chemistry either. However, the activated carbons E1 and E8 displayed a higher surface area and total pore volume than the activated carbon E5 (Table 3). Alike, E9 activated carbon stood out by its surface physical characteristics and high selectivity towards benzene (Tables 3 and 5); but it showed high content of acidic functional groups and low content of basic functional groups; so, it was assumed that its adsorption capacity was affected by its surface chemistry. Since the acidic surface groups provide hydrophilic sites that favor interaction with polar adsorbates (Boehm, 1994; Shen et al., 2010), it is believed that these groups repelled the adsorbates evaluated, hindering their diffusion inside the E9 material, which was reflected in the high values obtained for H_{MTZ} of this adsorbent. While the basics functional groups present on the surface of the E9 material favored π-π interactions with benzene, allowing higher adsorption of this hydrocarbon, and therefore high selectivity towards it; for this reason, during the separation of the binary mixture, all the cyclohexane initially adsorbed on the E9 material was displaced by the competitive action of benzene, achieving the separation of the cyclohexane/benzene mixture. These results confirmed that adsorption capacity was influenced by both the physical surface characteristics and the surface chemistry of these adsorbents.

3.3. Statistical analysis of the Taguchi experimental design

Result of S/N analysis to determine the preparation factors that had more influence on the benzene adsorption capacity of activated carbons during the separation of the binary mixture are presented in Table 6.

ANOVA is given in Table 7 and results showed that the most influential factors in the benzene adsorption capacity of activated carbons in the binary mixture separation were: the activating agent, ratio of impregnation, and physical activation time. The adsorbents E1, E4, E5, E6, and E8 showed the best S/N ratio. Fig. 7 illustrates the mean S/N ratio for tested conditions to prepare the activated carbons. Overall, the best conditions to prepare a coconut shell activated carbon with a high adsorption capacity for the separation of benzene from the binary mixture were: the activating agent at level 2 ($ZnCl_2$), activating agent concentration at level 2 (0.5 M), impregnation ratio at level 1 (1:2 m/v), and activation time with CO_2 at level 1 (2 h).

3.4. Best activated carbon for the benzene adsorption

The best activated carbon with the highest benzene adsorption capacity (QB) was prepared according to the preparation conditions established in Section 3.3. The results of its physicochemical characterization and adsorption performance are presented below.

Table 6
Results of S/N statistical analysis for the benzene adsorption in binary mixture using activated carbons prepared from coconut shell.

Activated carbon	Factor A*	Factor B*	Factor C*	Factor D*	q_t**	S/N
E1	CH_3COOH	1.0	1:2	2.0	27.01	28.6
E2	CH_3COOH	0.5	1:1	1.0	9.79	19.8
E3	CH_3COOH	0.1	1:0.5	0.5	4.84	13.7
E4	$ZnCl_2$	1.0	1:1	0.5	32.36	30.2
E5	$ZnCl_2$	0.5	1:0.5	2.0	28.96	29.2
E6	$ZnCl_2$	0.1	1:2	1.0	14.64	23.3
E7	H_3PO_4	1.0	1:0.5	1.0	1.35	2.6
E8	H_3PO_4	0.5	1:2	0.5	25.07	28.0
E9	H_3PO_4	0.1	1:1	2.0	6.91	16.8

*Factor A: Chemical agent; Factor B: Concentration of chemical agent (M); Factor C: Ratio (mass precursor/vol chemical agent); Factor D: Physical activation time (h) with CO_2 at 800 °C (h), **q_t: adsorption capacity (response variable).

Table 7
Results of ANOVA for the Taguchi experimental design used in the preparation of activated carbons for the separation of benzene.

Factor	Mean S/N ratio			Degrees of freedom (ν_F)	Sum of squares (SS)	Variance (σ_F)
	Level 1	Level 2	Level 3			
A: Activating agent	20.7	27.6	15.8	2	210.4	105.2
B: Activating agent concentration (%)	20.5	25.7	17.9	2	93.5	46.8
C: Impregnation ratio (m/v)	26.6	22.3	15.2	2	200.7	100.4
D: Activation time with CO_2 at 800 °C (h)	24.9	15.2	24.0	2	169.8	84.9
Error				0		
Total				8	674.4	

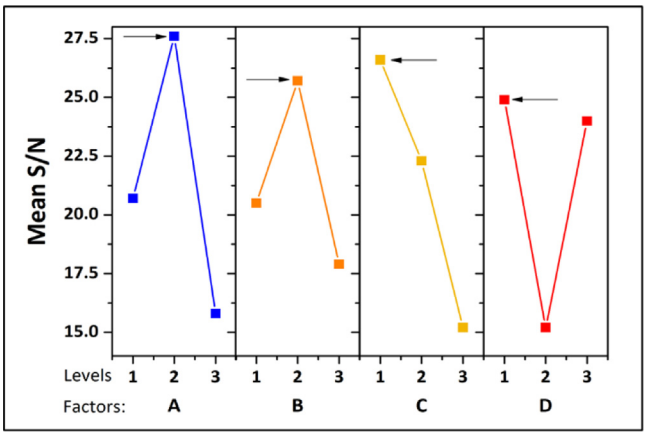

Fig. 7. Mean S/N ratio calculated for the benzene adsorption capacity of coconut shell activated carbons during the separation of the binary mixture benzene/cyclohexane. Arrows mark the levels with the highest mean S/N ratio (i.e., the best conditions to prepare the adsorbent).

3.4.1. Physicochemical characterization

Fig. 8-a shows the FT-IR spectrum of activated carbon QB. The comparison of this spectrum with the spectra of other activated carbons (Fig. 2) indicated some similarities and differences. The similarities included the absorption bands at 3700, 3400, 2920, 2850, 1730, and 1046 cm^{-1}; while the differences included the bands located at 1620, 1440, 1200, 1160, 1110, 720 and 590 cm^{-1}; as well as the region between 1620 and 1046 cm^{-1}. The sharp band at 1620 cm^{-1} was related to the stretching vibration of the C=C bond present in aromatic groups (Puziy et al., 2005). The band at 1440 cm^{-1} was assigned to the bending of the O-H bond present in carboxylic groups (Wang et al., 2015b; Foo and Hameed, 2012). The small band at 1200 cm^{-1} corresponded to the stretching of the C-O bond present in carboxylic groups (Wang et al., 2015b). The bands between 1160 and 1046 cm^{-1} were attributed to the stretching vibration of the C-O bond present in acids, alcohols, ethers, and esters (Saka, 2012). Bands below 1000 cm^{-1} were characteristic of the out-of-plane deformation of the C-H bond present in aromatic structures (Wang et al., 2015b). However, the bands between 700 and 590 can be also assigned to the bending of the O–C=O bond present in carboxylic groups. In summary, the broad band between 3700–3400 cm^{-1} and the bands at 1730, 1440, and 1200 cm^{-1} indicated the presence of carboxylic groups in the sample. So, it was inferred that carboxylic acids were the main functional groups on the surface of activated carbon QB.

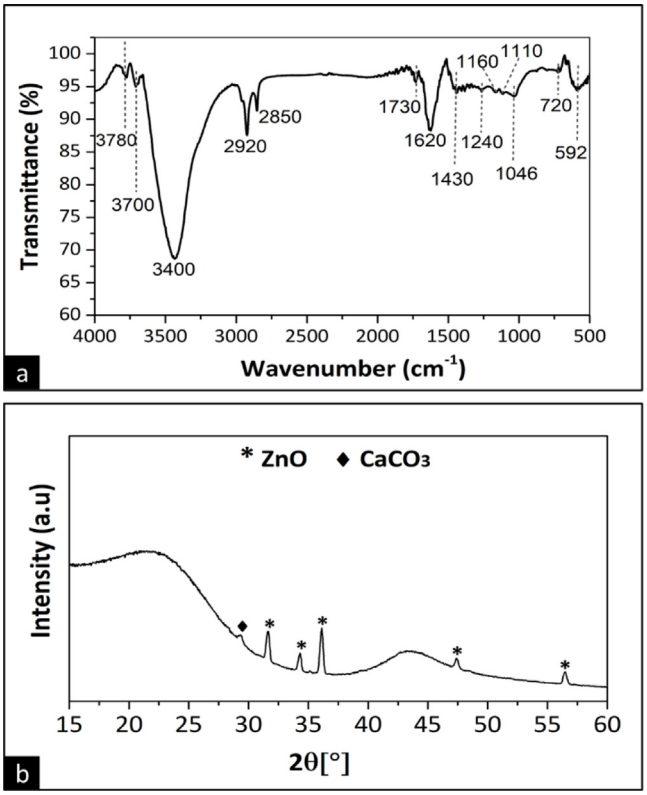

Fig. 8. (a) FT-IR spectrum and (b) X-ray diffraction pattern of the best activated carbon QB for benzene adsorption.

Table 8
Surface functional groups and PZC of the best activated carbon QB for benzene separation.

Functional groups	Carboxylic acids	Lactonic	Phenolic	Total acids	Total basics	PZC
Concentration (mmol/g)	0.017	–	–	0.017	0.562	6.8

Fig. 8-b shows the X-ray diffraction pattern of activated carbon QB. Peaks were observed at 31.69°, 34.38°, 36.18°, 47.45°, and 56.46°, which were attributed to the planes (100), (002), (101), (102) and (110) of the zinc oxide (ZnO, 01-079-0207). A weak peak was also observed at 29.40° that corresponded to the (104) plane of calcium carbonate ($CaCO_3$, 00-005-0586). Table 8 shows both the concentration of the acidic and basic surface functional groups, as well as the PZC of QB activated carbon. Carboxylic functionalities were the predominant acid functional groups on the surface of activated carbon QB thus confirming the FT-IR results. Furthermore, this adsorbent exhibited a basic surface character. Compared with the other activated carbons reported in Table 2, the adsorbent QB showed a lower total content of acidic functional groups; but it showed a lower total content of basic surface groups than those of activated carbons E2, E4, and E5, which also exhibited a basic surface character.

3.4.2. Evaluation of adsorption capacity and reuse cycles

Table 9 reports the calculated values of q_t, Ø, and H_{MTZ} for the adsorption of cyclohexane, benzene, and cyclohexane/benzene mixture using the activated carbon QB. This activated carbon showed a high adsorption capacity to separate benzene both in single and binary adsorption experiments. However, QB did not achieve a complete separation of the binary mixture because, after the adsorption process, benzene (corresponding to 93% of its adsorption capacity) and a small amount of cyclohexane (corresponding to 7% of its adsorption capacity) were retained on its surface.

The breakthrough curves of the adsorption of single and binary gases on activated carbon QB are shown in Fig. 9. The breakthrough time was reached in the first 6 min of the process for the adsorption of cyclohexane (Fig. 9-a) and 4 min after this operating condition, the adsorbent reached 80% of saturation. This adsorption process slowed down and reached the total saturation at 32.5 min. The slowdown of adsorption process can be related to the diffusion of the adsorbate in the mass transfer zone (i.e., low Ø and high H_{MTZ}). The displacement of cyclohexane was observed in the breakthrough curve of the binary adsorption (Fig. 9-b) due to the competitive effect of benzene as already described.

On the other hand, it is necessary to determine the life cycle or reusability of an adsorbent material because it determines its practical application and usage at an industrial level. Thus, four consecutive adsorption/desorption cycles

Table 9
Adsorption capacity of the best activated carbon QB for the separation of benzene.

Adsorption of monocomponent vapors						
Cyclohexane				Benzene		
q_t (mmol/g)	Ø	H_{MTZ} (cm)		q_t (mmol/g)	Ø	H_{MTZ} (cm)
13.68	0.17	2.33		40.32	0.37	1.55

Adsorption of binary mixture vapors							
Cyclohexane					Benzene		
q_{tc} (mmol/g)	q_f (mmol/g)	q_d (mmol/g)	Ø	H_{MTZ} (cm)	q_{tb} (mmol/g)	Ø	H_{MTZ} (cm)
6.99	2.63	4.36	0.43	0.94	33.10	0.46	1.72

q_{tc}: total amount of cyclohexane initially adsorbed, q_f: amount of cyclohexane remaining in the adsorbent, qd: amount of cyclohexane displaced to the effluent stream, q_{tb}: total amount of benzene adsorbed.

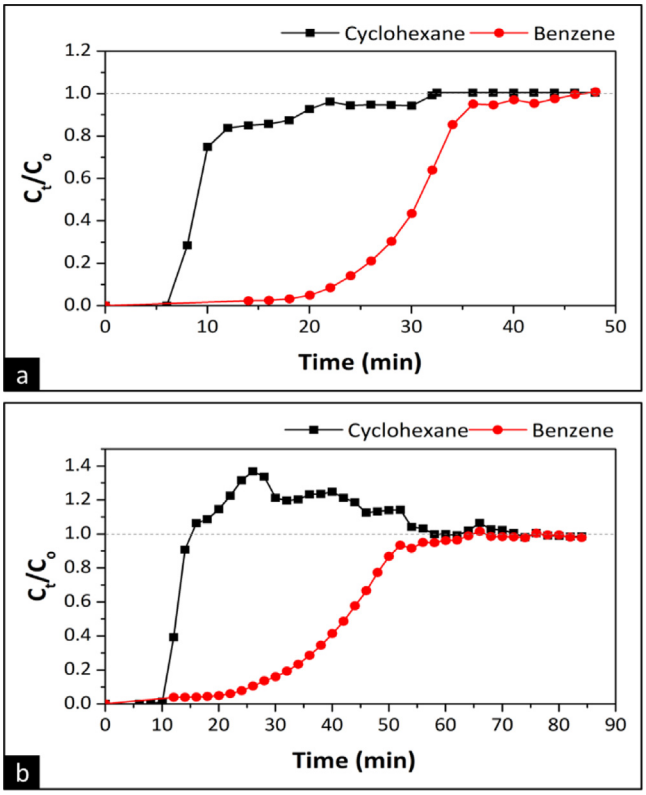

Fig. 9. Breakthrough curves for the adsorption of cyclohexane and benzene on the best activated carbon QB. (a) Monocomponent vapors and (b) bi-component vapors.

of the cyclohexane/benzene mixture were assessed to explore the reuse of activated carbon QB. Reusability experiments results are shown in Fig. 10. For the three consecutive adsorption/desorption cycles, the adsorbent QB retained its adsorption capacity at 100% in the adsorption/desorption of both hydrocarbons. After the third cycle of reuse, the adsorption capacity of this adsorbent maintained a reuse efficiency of approximately 96%. These results indicated that in the first three cycles, a very few amount of adsorbates remained on the QB surface after desorption. This could be attributed to the desorption temperature used was higher than the boiling points of both adsorbates, thus serving as a driving force for the desorption of the physisorbed molecules.

The reduction of adsorption capacity was ascribed to the incomplete desorption of the adsorbates, which can be caused by the formation of permanent bonds between the adsorbent and adsorbate molecules and pore blockage. The incomplete regeneration of the activated carbon QB can be attributed to the residual content of the physisorbed benzene, because this compound had a strong affinity for the adsorbent (Fig. 9-b). Note that its residual content could condense inside the pores and block pores, making desorption difficult and compromising the adsorption capacity of the activated carbon QB.

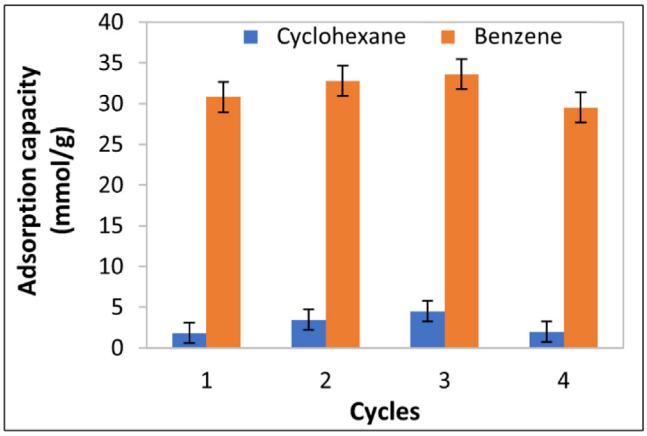

Fig. 10. Regeneration studies for the adsorption–desorption of cyclohexane/benzene mixture on the best activated carbon QB.

Overall, the activated carbon QB showed good reusability and could be used as an efficient and regenerable adsorbent for cyclohexane/benzene mixture separation.

3.5. Comparison with other studies published in the literature

A systematic review was carried out to compare the adsorption capacity of the activated carbons obtained in this study with other studies published in the literature. For this comparison, the selectivity was calculated as the ratio between the benzene adsorption capacity and the cyclohexane adsorption capacity of the adsorbent. According to the results shown in Table 10, the functionalized mesoporous silicas synthesized by Dou et al. (2011) and Hu et al. (2009) presented lower selectivity and adsorption capacity than the activated carbons prepared in this study. SBA-2 mesoporous silicas (240 °C and 550 °C) reported by Emparan-Legaspi et al. (2020) registered a higher selectivity towards benzene than the other materials; however, their adsorption capacity and surface area were lower than those of the activated carbons of this study. Likewise, the MOFs reported by Sapianik et al. (2020), Santra et al. (2017), Zhang et al. (2016), Mukherjee et al. (2016), Manna et al. (2015), and Ma et al. (2011) showed a lower adsorption capacity than the activated carbons of this study for single adsorbates. Also, Hijikata et al. (2011) reported a MOF (CID-23) with high adsorption capacity, which was measured by adsorption isotherms; but only the adsorbent ability to separate the vapors from the binary mixture in a batch adsorption system was reported. Wang et al. (2015a) reported an ordered mesoporous carbon with a high adsorption capacity for the monocomponent gas; but its capability to separate the cyclohexane/benzene mixture using a dynamic adsorption system was not evaluated.

Note that a low adsorption capacity implies using a significant quantity of adsorbent to achieve the separation target, which would not be economically profitable with ordered mesoporous silicas or MOF reported in Table 10, because their production processes involve expensive raw materials. Low-cost and reusable adsorbents with high selectivity and high adsorption capacity are needed to separate the cyclohexane/benzene mixture. In this sense, the activated carbons E5 and QB are good alternatives, because they presented high benzene adsorption capacity. Additionally, the adsorbent E5 showed high selectivity and allowed the total separation of the binary mixture; while the activated carbon QB allowed an acceptable separation and presented good reusability. Besides, the production process of these activated carbons provides advantages in terms of cost-effectiveness, especially when organic residues are used as raw precursors.

4. Conclusions

New activated carbons for the separation of benzene and cyclohexane were prepared from the coconut shell by a Taguchi experimental design. Adsorption properties of these activated carbons were analyzed and the best preparation conditions were identified to improve their separation performance for the separation of the cyclohexane/benzene mixture. ANOVA analysis of the Taguchi design indicated that the most influential factors for the preparation of the coconut shell activated carbons to improve the benzene adsorption in binary mixture separation were: the activating agent, ratio of impregnation, and physical activation time. The best preparation conditions of coconut shell activated carbon were determined, which provided the highest benzene adsorption capacity. This adsorbent allowed an acceptable separation of this mixture (i.e., 92.64%: benzene and 7.36%: cyclohexane) and showed a reuse efficiency of 96% after four consecutive adsorption/desorption cycles.

Table 10
Comparative of adsorbents reported for the separation of benzene and cyclohexane.

Adsorbent material	Monocomponent adsorption (mmol/g)		Binary mixture adsorption (mmol/g)		Selectivity (q_b/q_c)	Surface area (m^2/g)	Reference
	C_6H_{12}	C_6H_6	C_6H_{12}	C_6H_6			
E1 activated carbon	8.41	33.95	4.78	27.01	5.65	658.31	
E4 activated carbon	25.2	51.40	12.83	32.36	2.52	894.05	2021
E5 activated carbon	4.72	32.44	2.61	28.96	11.1	637.47	This study
E8 activated carbon	8.59	32.48	4.63	25.07	5.41	808.04	
QB activated carbon	13.68	40.32	6.99	33.10	4.73	–	
1-H (MOF)	2.8	3.9	–	–	–	1050–1135	2020
1-Br (MOF)	2.0	2.7	–	–	–	855–876	Sapianik
1-NO2 (MOF)	0.2	2.9	–	–	–	742–800	et al. (2020)
1-NH2 (MOF)	2.0	3.2	–	–	–	431–446	
SBA-2 (240 °C)	0.164	1.743	0.008	1.19	148.75	314.81	2020
SBA-2 (550 °C)	0.065	0.713	0.0006	0.443	738.33	337.92	Emparan-Legaspi
SBA-2 (800 °C)	0.039	0.22	0.0197	0.044	2.23	139.83	et al. (2020)
ZMF (Reticulated foam)	2.5	4.5	–	–	–	957	2017 Saini and Pires (2017)
MOF 1	0.06	2.7	–	–	–	–	2017 Santra et al. (2017)
MFOF-1 (MOF)	2.02	4.5	–	–	–	2287	2016 Zhang et al. (2016)
Mg-MOF-74	0.4	8.15	–	–	–		
Mn-MOF-74	0.25	9.38	–	–	–		
Fe-MOF-74	0.15	5.5	–	–	–		2016
Co-MOF-74	0.23	5.57	–	–	–	1500–1600	Mukherjee
Ni-MOF-74	0.09	9.19	–	–	–		et al.
Cu-MOF-74	0.13	7.55	–	–	–		(2016)
Zn-MOF-74	0.17	6.76	–	–	–		
DAT-MOF-1	0.2	1.5	–	–	–	–	2015 Manna et al. (2015)
Ordered mesoporous carbon	14.19	17.34	–	–	–	1762	2015 Wang et al. (2015a)
NENU-28	1.70	3.42	–	–	–	470	2011
NENU-29	1.64	3.38	–	–	–	466	Ma
NENU-3	1.58	3.29	–	–	–	405	et al.
$Cu_3(BTC)_2$	1.48	3.21	–	–	–	1507	(2011)
CID-23 (MOF)	18.5	303	–	–	–	553	2011 Hijikata et al. (2011)
SBA-15		0.91	0.32	0.54	1.69	698	
p-SBA-15		0.65	0.24	0.4	1.67	506	
MCM-41		1.02	0.36	0.57	1.58	1088	2011
p-MCM-41		0.9	0.2	0.54	2.70	950	Dou
MCM-48		0.98	0.37	0.58	1.57	1210	et al.
p-MCM-48		0.78	0.21	0.55	2.62	1164	(2011)
KIT-6		1.26	0.32	0.67	2.09	912	
p-KIT-6		1.17	0.34	0.69	2.03	751	
Pure SBA-15		0.292	0.16	0.34	2.13	501	
(1:20)MTES		0.36	–	–	–	512	
(1:10)MTES		0.418	–	–	–	577.1	2009
(1:5)MTES		0.283	–	–	–	611.4	Hu
(1:20)PTES		0.478	0.189	0.419	2.22	637.5	et al.
(1:15)PTES		0.632	0.33	0.524	1.59	692.4	(2009)
(1:10)PTES		0.65	0.285	0.449	1.58	794.5	
(1:5)PTES		0.626	0.193	0.433	2.24	645.6	

CRediT authorship contribution statement

Aniyohana Valencia: Investigation, Methodology, Writing – original draft. **Roberto Muñiz-Valencia:** Methodology, Supervision, Writing – review & editing. **Silvia G. Ceballos-Magaña:** Conceptualization, Validation. **Cintia Karina Rojas-Mayorga:** Conceptualization, Validation. **Adrian Bonilla-Petriciolet:** Resources, Methodology. **Jorge González:** Methodology. **Ismael Alejandro Aguayo-Villarreal:** Conceptualization, Visualization, Funding acquisition.

Declaration of competing interest

The authors declare that they have no known competing financial interests or personal relationships that could have appeared to influence the work reported in this paper.

Acknowledgments

This work was supported by Consejo-Nacional-de-Ciencia-y-Tecnología (México) (A1-S-10035) and Secretaría de Educación Publica (México) (UCOL-PTC-255). Aniyohana acknowledges to the Consejo-Nacional-de-Ciencia-y-Tecnología (México) the financial support provided through the scholarship (CVU 783578).

References

Afrane, G., Achaw, O.-W., 2008. Effect of the concentration of inherent mineral elements on the adsorption capacity of coconut shell-based activated carbons. Bioresour. Technol. 99, 6678–6682. http://dx.doi.org/10.1016/j.biortech.2007.11.071.

Aguayo-Villarreal, I.A., Bonilla-Petriciolet, A., Muñiz-Valencia, R., 2017a. Preparation of activated carbons from pecan nutshell and their application in the antagonistic adsorption of heavy metal ions. J. Mol. Liquids 230, 686–695. http://dx.doi.org/10.1016/j.molliq.2017.01.039.

Aguayo-Villarreal, I.A., Montes-Morán, M.A., Hernández-Montoya, V., Bonilla-Petriciolet, A., Concheso, A., Rojas-Mayorga, C.K., González, J., 2017b. Importance of iron oxides on the carbons surface vs the specific surface for VOC's adsorption. Ecol. Eng. 106, 400–408. http://dx.doi.org/10.1016/j.ecoleng.2017.05.043.

Ahmad, M., Rajapaksha, A.U., Lim, J.E., Zhang, M., Bolan, N., Mohan, D., Vithanage, M., Lee, S.S., Ok, Y.S., 2014. Biochar as a sorbent for contaminant management in soil and water: A review. Chemosphere 99, 19–33. http://dx.doi.org/10.1016/j.chemosphere.2013.10.071.

Ahmedna, M., Marshall, W.E., Rao, R.M., 2000. Production of granular activated carbons from select agricultural by-products and evaluation of their physical, chemical and adsorption properties1Louisiana Agricultural Experiment Station manuscript 99-21-0066.1. Bioresour. Technol. 71, 113–123. http://dx.doi.org/10.1016/S0960-8524(99)00070-X.

Boehm, H.P., 1994. Some aspects of the surface chemistry of carbon blacks and other carbons. Carbon 32, 759–769. http://dx.doi.org/10.1016/0008-6223(94)90031-0.

Boehm, H.P., 2002. Surface oxides on carbon and their analysis: a critical assessment. Carbon 40, 145–149. http://dx.doi.org/10.1016/S0008-6223(01)00165-8.

Dada, E.A., Achenie, L., 2012. Production of cylohexane from hydrogenation of benzene using microreactor technology. In: Karimi, I.A., Srinivasan, R. (Eds.), Computer Aided Chemical Engineering. Elsevier, pp. 240–244. http://dx.doi.org/10.1016/B978-0-444-59507-2.50040-8.

Danish, M., Ahmad, T., 2018. A review on utilization of wood biomass as a sustainable precursor for activated carbon production and application. Renew. Sustain. Energy Rev. 87, 1–21. http://dx.doi.org/10.1016/j.rser.2018.02.003.

Dou, B., Hu, Q., Li, J., Qiao, S., Hao, Z., 2011. Adsorption performance of VOCs in ordered mesoporous silicas with different pore structures and surface chemistry. J. Hazard. Mater. 186, 1615–1624. http://dx.doi.org/10.1016/j.jhazmat.2010.12.051.

Elizalde-González, M.P., Hernández-Montoya, V., 2009. Removal of acid orange 7 by guava seed carbon: A four parameter optimization study. J. Hazard. Mater. 168, 515–522. http://dx.doi.org/10.1016/j.jhazmat.2009.02.064.

Emparan-Legaspi, M.J., Gonzalez, J., Gonzalez-Carrillo, G., Ceballos-Magaña, S.G., Canales-Vazquez, J., Aguayo-Villarreal, I.A., Muñiz Valencia, R., 2020. Dynamic adsorption separation of benzene/cyclohexane mixtures on micro-mesoporous silica SBA-2. Microporous Mesoporous Mater. 294, 109942. http://dx.doi.org/10.1016/j.micromeso.2019.109942.

Foo, K.Y., Hameed, B.H., 2012. Coconut husk derived activated carbon via microwave induced activation: Effects of activation agents, preparation parameters and adsorption performance. Chem. Eng. J. 184, 57–65. http://dx.doi.org/10.1016/j.cej.2011.12.084.

Gabelman, A., 2017. Adsorption basics: part 1. Chem. Eng. Progr. 113, 48–53.

Gil, R.R., Ruiz, B., Lozano, M.S., Martín, M.J., Fuente, E., 2014. VOCs removal by adsorption onto activated carbons from biocollagenic wastes of vegetable tanning. Chem. Eng. J. 245, 80–88. http://dx.doi.org/10.1016/j.cej.2014.02.012.

Goertzen, S.L., Thériault, K.D., Oickle, A.M., Tarasuk, A.C., Andreas, H.A., 2010. Standardization of the Boehm titration. Part I. CO2 expulsion and endpoint determination. Carbon 48, 1252–1261. http://dx.doi.org/10.1016/j.carbon.2009.11.050.

González-García, P., 2018. Activated carbon from lignocellulosics precursors: A review of the synthesis methods, characterization techniques and applications. Renew. Sustain. Energy Rev. 82, 1393–1414. http://dx.doi.org/10.1016/j.rser.2017.04.117.

Guo, Z., Huang, J., Xue, Z., Wang, X., 2016. Electrospun graphene oxide/carbon composite nanofibers with well-developed mesoporous structure and their adsorption performance for benzene and butanone. Chem. Eng. J. 306, 99–106. http://dx.doi.org/10.1016/j.cej.2016.07.048.

Hadi, P., Xu, M., Ning, C., Sze Ki Lin, C., McKay, G., 2015. A critical review on preparation, characterization and utilization of sludge-derived activated carbons for wastewater treatment. Chem. Eng. J. 260, 895–906. http://dx.doi.org/10.1016/j.cej.2014.08.088.

He, X., Ling, P., Yu, M., Wang, X., Zhang, X., Zheng, M., 2013. Rice husk-derived porous carbons with high capacitance by Zncl2 activation for supercapacitors. Electrochim. Acta 105, 635–641. http://dx.doi.org/10.1016/j.electacta.2013.05.050.

Hernández-Hernández, L.E., Bonilla-Petriciolet, A., Mendoza-Castillo, D.I., Reynel-Ávila, H.E., 2017. Antagonistic binary adsorption of heavy metals using stratified bone char columns. J. Mol. Liquids 241, 334–346. http://dx.doi.org/10.1016/j.molliq.2017.05.148.

Hijikata, Y., Horike, S., Sugimoto, M., Sato, H., Matsuda, R., Kitagawa, S., 2011. Relationship between channel and sorption properties in coordination polymers with interdigitated structures. Chem. – Eur. J. 17, 5138–5144. http://dx.doi.org/10.1002/chem.201003734.

Hong, D., Zhou, J., Hu, C., Zhou, Q., Mao, J., Qin, Q., 2019. Mercury removal mechanism of AC prepared by one-step activation with ZnCl2. Fuel 235, 326–335. http://dx.doi.org/10.1016/j.fuel.2018.07.103.

Hu, Q., Li, J.J., Hao, Z.P., Li, L.D., Qiao, S.Z., 2009. Dynamic adsorption of volatile organic compounds on organofunctionalized SBA-15 materials. Chem. Eng. J. 149, 281–288. http://dx.doi.org/10.1016/j.cej.2008.11.003.

Ioannidou, O., Zabaniotou, A., 2007. Agricultural residues as precursors for activated carbon production—A review. Renew. Sustain. Energy Rev. 11, 1966–2005. http://dx.doi.org/10.1016/j.rser.2006.03.013.

Kumarasinghe, K., Kumara, G.R.A., Rajapakse, R.M.G., Liyanage, D.N., Tennakone, K., 2019. Activated coconut shell charcoal based counter electrode for dye-sensitized solar cells. Organ. Electron. 71, 93–97. http://dx.doi.org/10.1016/j.orgel.2019.05.009.

Lee, T., Zubir, Z.A., Jamil, F.M., Matsumoto, A., Yeoh, F.-Y., 2014. Combustion and pyrolysis of activated carbon fibre from oil palm empty fruit bunch fibre assisted through chemical activation with acid treatment. J. Anal. Appl. Pyrol. 110, 408–418. http://dx.doi.org/10.1016/j.jaap.2014.10.010.

Li, B., 2012. Charaterization of pore structure and surface chemistry of activated carbons – a review. Fourier Transf. - Mater. Anal. http://dx.doi.org/10.5772/37460.

Li, W., Xu, B., Lei, Z., Dai, C., 2018. Separation of benzene and cyclohexane by extractive distillation intensified with ionic liquid. Chem. Eng. Process. - Process Intensif. 126, 81–89. http://dx.doi.org/10.1016/j.cep.2018.02.016.
Liyanage, C.D., Pieris, M., 2015. A physico-chemical analysis of coconut shell powder. Procedia Chem. 16, 222–228. http://dx.doi.org/10.1016/j.proche.2015.12.045.
Long, X., Duan, B., Cao, H., Jia, M., Wu, L., 2018. Removal of NO with the hexamminecobalt(II) solution catalyzed by the activated carbon treated with acetic acid. J. Ind. Eng. Chem. 62, 217–224. http://dx.doi.org/10.1016/j.jiec.2017.12.060.
Lu, J., Wu, X., Li, Y., Cui, W., Liang, Y., 2018. Modified silica gel surface with chelating ligand for effective mercury ions adsorption. Surf. Interfaces. 12, 108–115. http://dx.doi.org/10.1016/j.surfin.2018.04.005.
Ma, F.-J., Liu, S.-X., Liang, D.-D., Ren, G.-J., Wei, F., Chen, Y.-G., Su, Z.-M., 2011. Adsorption of volatile organic compounds in porous metal–organic frameworks functionalized by polyoxometalates. J. Solid State Chem. 184, 3034–3039. http://dx.doi.org/10.1016/j.jssc.2011.09.002.
Maciá-Agulló, J.A., Moore, B.C., Cazorla-Amorós, D., Linares-Solano, A., 2004. Activation of coal tar pitch carbon fibres: Physical activation vs. chemical activation. Carbon 42, 1367–1370. http://dx.doi.org/10.1016/j.carbon.2004.01.013.
Maitlo, H.A., Kim, K.-H., Khan, A., Szulejko, J.E., Kim, J.C., Song, H.N., Ahn, W.-S., 2019. Competitive adsorption of gaseous aromatic hydrocarbons in a binary mixture on nanoporous covalent organic polymers at various partial pressures. Environ. Res. 173, 1–11. http://dx.doi.org/10.1016/j.envres.2019.03.028.
Manna, B., Mukherjee, S., Desai, A.V., Sharma, S., Krishna, R., Ghosh, S.K., 2015. A π-electron deficient diaminotriazine functionalized MOF for selective sorption of benzene over cyclohexane. Chem. Commun. 51, 15386–15389. http://dx.doi.org/10.1039/C5CC06128H.
Mohammed, J., Nasri, N.S., Ahmad Zaini, M.A., Hamza, U.D., Ani, F.N., 2015. Adsorption of benzene and toluene onto KOH activated coconut shell based carbon treated with NH3. Int. Biodeterioration Biodegrad. 102, 245–255. http://dx.doi.org/10.1016/j.ibiod.2015.02.012.
Mukherjee, S., Manna, B., Desai, A.V., Yin, Y., Krishna, R., Babarao, R., Ghosh, S.K., 2016. Harnessing lewis acidic open metal sites of metal–organic frameworks: the foremost route to achieve highly selective benzene sorption over cyclohexane. Chem. Commun. (Camb). 52, 8215–8218. http://dx.doi.org/10.1039/c6cc03015g.
Nasiruddin Khan, M., Sarwar, A., 2007. Determination of points of zero charge of natural and treated adsorbents. Surf. Rev. Lett. 14, 461–469. http://dx.doi.org/10.1142/S0218625X07009517.
Nieto-Delgado, C., Rangel-Mendez, J.R., 2011. Production of activated carbon from organic by-products from the alcoholic beverage industry: Surface area and hardness optimization by using the response surface methodology. Ind. Crops Prod. 34, 1528–1537. http://dx.doi.org/10.1016/j.indcrop.2011.05.014.
Pak, S.-H., Jeon, M.-J., Jeon, Y.-W., 2016. Study of sulfuric acid treatment of activated carbon used to enhance mixed VOC removal. Int. Biodeterioration Biodegrad. 113, 195–200. http://dx.doi.org/10.1016/j.ibiod.2016.04.019.
Prahas, D., Kartika, Y., Indraswati, N., Ismadji, S., 2008. Activated carbon from jackfruit peel waste by H3PO4 chemical activation: Pore structure and surface chemistry characterization. Chem. Eng. J. 140, 32–42. http://dx.doi.org/10.1016/j.cej.2007.08.032.
Puziy, A.M., Poddubnaya, O.I., Martínez-Alonso, A., Suárez-García, F., Tascón, J.M.D., 2005. Surface chemistry of phosphorus-containing carbons of lignocellulosic origin. Carbon 43, 2857–2868. http://dx.doi.org/10.1016/j.carbon.2005.06.014.
Radovic, L.R., Silva, I.F., Ume, J.I., Menéndez, J.A., Leon, C.A.L.Y., Scaroni, A.W., 1997. An experimental and theoretical study of the adsorption of aromatics possessing electron-withdrawing and electron-donating functional groups by chemically modified activated carbons. Carbon 35, 1339–1348. http://dx.doi.org/10.1016/S0008-6223(97)00072-9.
Radovic, L.R., Ume, J.I., Scaroni, A.W., 1996. On tailoring the surface chemistry of activated carbons for their use in purification of aqueous effluents. In: LeVan, M.D. (Ed.), Fundamentals of Adsorption: Proceedings of the Fifth International Conference on Fundamentals of Adsorption. Springer US, Boston, MA, pp. 749–756. http://dx.doi.org/10.1007/978-1-4613-1375-5_93.
Ramirez-Gutierrez, C.F., Arias-Niquepa, R., Prías-Barragán, J.J., Rodriguez-Garcia, M.E., 2020. Study and identification of contaminant phases in commercial activated carbons. J. Environ. Chem. Eng. 8, 103636. http://dx.doi.org/10.1016/j.jece.2019.103636.
Rashidi, N.A., Yusup, S., 2017. A review on recent technological advancement in the activated carbon production from oil palm wastes. Chem. Eng. J. 314, 277–290. http://dx.doi.org/10.1016/j.cej.2016.11.059.
Raveendran, K., Ganesh, A., Khilar, K.C., 1995. Influence of mineral matter on biomass pyrolysis characteristics. Fuel 74, 1812–1822. http://dx.doi.org/10.1016/0016-2361(95)80013-8.
Ribeiro, C.P., Freeman, B.D., Kalika, D.S., Kalakkunnath, S., 2012. Aromatic polyimide and polybenzoxazole membranes for the fractionation of aromatic/aliphatic hydrocarbons by pervaporation. J. Membr. Sci. 390–391, 182–193. http://dx.doi.org/10.1016/j.memsci.2011.11.042.
Saini, V.K., Pires, J., 2017. Development of metal organic framework-199 immobilized zeolite foam for adsorption of common indoor VOCs. J. Environ. Sci. 55, 321–330. http://dx.doi.org/10.1016/j.jes.2016.09.017.
Saka, C., 2012. BET, TG–DTG, FT-IR, SEM, iodine number analysis and preparation of activated carbon from acorn shell by chemical activation with ZnCl2. J. Anal. Appl. Pyrol. 95, 21–24. http://dx.doi.org/10.1016/j.jaap.2011.12.020.
Salame, I.I., Bandosz, T.J., 2001. Surface chemistry of activated carbons: Combining the results of temperature-programmed desorption, boehm, and potentiometric titrations. J. Colloid Interface Sci. 240, 252–258. http://dx.doi.org/10.1006/jcis.2001.7596.
Salleh, M.Z.M., Hadj-Kali, M.K., Hashim, M.A., Mulyono, S., 2018. Ionic liquids for the separation of benzene and cyclohexane – COSMO-RS screening and experimental validation. J. Mol. Liquids 266, 51–61. http://dx.doi.org/10.1016/j.molliq.2018.06.034.
Salleh, Z., Wazeer, I., Mulyono, S., El-blidi, L., Hashim, M.A., Hadj-Kali, M.K., 2017. Efficient removal of benzene from cyclohexane-benzene mixtures using deep eutectic solvents – COSMO-RS screening and experimental validation. J. Chem. Thermodynam. 104, 33–44. http://dx.doi.org/10.1016/j.jct.2016.09.002.
Santra, A., Francis, M., Parshamoni, S., Konar, S., 2017. Nanoporous Cu(I) metal–organic framework: Selective adsorption of benzene and luminescence sensing of nitroaromatics. ChemistrySelect 2, 3200–3206. http://dx.doi.org/10.1002/slct.201700416.
Sapianik, A.A., Kovalenko, K.A., Samsonenko, D.G., Barsukova, M.O., Dybtsev, D.N., Fedin, V.P., 2020. Exceptionally effective benzene/cyclohexane separation using a nitro-decorated metal–organic framework. Chem. Commun. 56, 8241–8244. http://dx.doi.org/10.1039/D0CC03227A.
Seung Kim, Y., Rae Park, C., 2016. Titration method for the identification of surface functional groups. In: Inagaki, M., Kang, F. (Eds.), Materials Science and Engineering of Carbon. Butterworth-Heinemann, pp. 273–286. http://dx.doi.org/10.1016/B978-0-12-805256-3.00013-1, Chapter 13.
Shen, W., Li, Z., Liu, Y., 2010. Surface chemical functional groups modification of porous carbon. Recent Patents Chem. Eng. 1, 27–40. http://dx.doi.org/10.2174/1874478810801010027.
Shin, H.-G., Kim, H., Noh, T., Kim, D., Kim, Y.-N., 2011. Degradation behavior of high surface area calcium hydroxide sorbent for SO2 removal. Int. J. Min. Process. 98, 145–149. http://dx.doi.org/10.1016/j.minpro.2010.11.002.
Son, H.K., Sivakumar, S., Rood, M.J., Kim, B.J., 2016. Electrothermal adsorption and desorption of volatile organic compounds on activated carbon fiber cloth. J. Hazard. Mater. 301, 27–34. http://dx.doi.org/10.1016/j.jhazmat.2015.08.040.
Sui, H., Liu, J., He, L., Li, X., Jani, A., 2019. Adsorption and desorption of binary mixture of acetone and ethyl acetate on silica gel. Chem. Eng. Sci. 197, 185–194. http://dx.doi.org/10.1016/j.ces.2018.12.010.
Sun, L., Liu, J., Luo, W., Yang, Y., Wang, F., Weerakkody, C., Suib, S.L., 2018. Preparation of amorphous copper - chromium oxides catalysts for selective oxidation of cyclohexane. Mol. Catal. 460, 16–26. http://dx.doi.org/10.1016/j.mcat.2018.09.007.

Thommes, M., Kaneko, K., Neimark, A.V., Olivier, J.P., Rodriguez-Reinoso, F., Rouquerol, J., Sing, K.S.W., 2015. Physisorption of gases, with special reference to the evaluation of surface area and pore size distribution (IUPAC Technical Report). Pure Appl. Chem. 87, 1051–1069. http://dx.doi.org/10.1515/pac-2014-1117.

Wang, G., Dou, B., Zhang, Z., Wang, J., Liu, H., Hao, Z., 2015a. Adsorption of benzene, cyclohexane and hexane on ordered mesoporous carbon. J. Environ. Sci. 30, 65–73. http://dx.doi.org/10.1016/j.jes.2014.10.015.

Wang, R., Li, C., Meng, H., Wang, J., Wang, Z., 2008. Ternary liquid-liquid equilibria measurement for benzene + cyclohexane + N-methylimidazole, or N-ethylimidazole, or N-methylimidazolium dibutylphosphate at 298.2 K and atmospheric pressure. J. Chem. Eng. Data. 53, 2170–2174. http://dx.doi.org/10.1021/je800376f.

Wang, H., Sun, Y., Zhu, T., Wang, W., Deng, H., 2015b. Adsorption of acetaldehyde onto carbide-derived carbon modified by oxidation. Chem. Eng. J. 273, 580–587. http://dx.doi.org/10.1016/j.cej.2015.03.107.

Yahya, M.A., Al-Qodah, Z., Ngah, C.W.Z., 2015. Agricultural bio-waste materials as potential sustainable precursors used for activated carbon production: A review. Renew. Sustain. Energy Rev. 46, 218–235. http://dx.doi.org/10.1016/j.rser.2015.02.051.

Yang, R.T., 2003. Introductory remarks. In: Adsorbents: Fundamentals and Applications. John Wiley & Sons, Inc., Hoboken, NJ, USA, pp. 1–7. http://dx.doi.org/10.1002/047144409X, (Chapter 1).

Yuen, F.K., Hameed, B.H., 2009. Recent developments in the preparation and regeneration of activated carbons by microwaves. Adv. Colloid Interface Sci. 149, 19–27. http://dx.doi.org/10.1016/j.cis.2008.12.005.

Zhang, X., Gao, B., Creamer, A.E., Cao, C., Li, Y., 2017. Adsorption of VOCs onto engineered carbon materials: A review. J. Hazard. Mater. 338, 102–123. http://dx.doi.org/10.1016/j.jhazmat.2017.05.013.

Zhang, G., Liu, Y., Zheng, S., Hashisho, Z., 2019. Adsorption of volatile organic compounds onto natural porous minerals. J. Hazard. Mater. 364, 317–324. http://dx.doi.org/10.1016/j.jhazmat.2018.10.031.

Zhang, L., Yang, W., Wu, X.-Y., Lu, C.-Z., Chen, W.-Z., 2016. A Hydrophobic Metal–Organic Framework Based on Cubane-type [Co4(μ3-F)3(μ3-SO4)]3+ clusters for gas storage and adsorption selectivity of benzene over cyclohexane. Chem. Eur. J. 22, 11283–11290. http://dx.doi.org/10.1002/chem.201600705.

Zhao, X., Zeng, X., Qin, Y., Li, X., Zhu, T., Tang, X., 2018. An experimental and theoretical study of the adsorption removal of toluene and chlorobenzene on coconut shell derived carbon. Chemosphere 206, 285–292. http://dx.doi.org/10.1016/j.chemosphere.2018.04.126.